Photosystem II monomeric antenna CP26 has a key role in Non-Photochemical Quenching in *Chlamydomonas reinhardtii*

Stefano Cazzaniga[1], Minjae Kim[2], Matteo Pivato[1], Federico Perozeni[1], Samim Sardar[3], Cosimo D'Andrea[3,4], EonSeon Jin[2*], Matteo Ballottari[1*]

[1] *Dipartimento di Biotecnologie, Università di Verona, Verona, Italy*

[2] *Department of Life Science, Research Institute for Natural Sciences, Hanyang University, Seoul, South Korea*

[3] *Istituto Italiano di Tecnologia, Center for Nano Science and Technology, Milano, Italy*

[4] *Dipartimento di Fisica, Politecnico di Milano, Milano, Italy*

**Corresponding authors: Matteo Ballottari, Dipartimento di Biotecnologie, Università di Verona, Strada le Grazie 15, 37134 Verona Italy; E-mail:* matteo.ballottari@univr.it; *EonSeon Jin, Department of Life Science, Hanyang University, Seoul, South Korea* esjin@hanyang.ac.kr

Running head: Role of CP26 in photoprotection in *Chlamydomonas*

ABSTRACT

Eukaryotic photosynthetic organisms have evolved an array of "antenna" complexes where both light harvesting and photoprotective mechanisms occur. Thermal dissipation of the excitation energy harvested in excess, named non-photochemical quenching (NPQ), is one of the main photoprotective mechanisms evolved in eukaryotic organisms to prevent photooxidative stress. Here, the role of the Photosystem II monomeric antenna CP26 was investigated in *Chlamydomonas reinhardtii,* model organism for green algae, using a genome editing approach to obtain *cp26* knock-out mutant strains (named *k6*). The absence of CP26 caused a reduced growth at low or medium light but not at high irradiances. Photosystem II were partially affected by the absence of CP26 having reduced photochemical efficiency, light harvesting capacity and excitation energy transfer. However, the main phenotype observed in *k6* was a strong reduction of NPQ, being reduced by more than 70% compared to wild type. The NPQ phenotype observed was rescued by genetic complementation of *k6* mutant demonstrating that ~50% of CP26 content compared to wild type was able to restore the NPQ capacity. The comparison of *k6* mutant with mutants deprived of the other Photosystem II monomeric antenna, CP29 or missing both CP26 and CP29, demonstrated that these monomeric antenna proteins have different specific functions in *Chlamydomonas reinhardtii:* CP26 plays a

pivotal role in NPQ induction while the binding of CP29 to Photosystem II is crucial for its photochemical activity. The genetic engineering of these two proteins could be a promising strategy to regulate photosynthetic efficiency of microalgae under different light regimes.

INTRODUCTION

Photosynthetic complexes absorb photons and transfer electrons to the redox reactions, leading to the synthesis of NADPH and ATP used to fix CO_2 into organic molecules (Hill and Scarisbrick, 1940). Chlorophyll (Chl) and carotenoids (Car) are the molecules responsible for capturing light radiation. Pigments light absorption takes place in the photosynthetic apparatus, localized in the thylakoid membranes and composed of four multiproteic complexes: photosystem II (PSII), cytochrome *b6f,* photosystem I (PSI) and ATP synthase (Nelson and Ben Shem, 2004). The two photosystems are organized into two major moieties: reaction center (RC) and antenna subunits (Suga et al., 2015). Light-harvesting antenna proteins allow to increase the rate of light energy capturing, efficiently transferring the excitation energy to the RC (Croce and Van Amerongen, 2011). In limiting light conditions, this increased energy capturing is crucial to maximize ATP and NADPH production, required for CO_2 fixation. However, increased light harvesting capacity may become a potential source of harmful effects upon exposure to high light (Long et al., 1994). An excessive light irradiance causes the saturation of the electron transport chain and overload of RCs, blocking or limiting the forward electron transport and preventing the photochemical use of the received energy. Limitation at the acceptor side can extend the lifetime of excited Chls, increasing the probability of generating their triplet states. Triplets, in turn, can react with oxygen, causing the formation of reactive oxygen species (ROS) and leading to photodamage (Neidhardt et al., 1998). PSII RC components are particularly sensitive to photodamage (Vass et al., 1992) with a specific repair cycle allowing to replace the damaged RC in the membrane (Aro et al., 1993). Photodamage can be related to excessive light, but also to variable environmental conditions, that could cause sudden changes in light irradiation (sun flecks), rapidly changing the number of photons received and transiently overload the RCs (Graham et al., 2017). Moreover, possible overload of the photosynthetic apparatus can be a consequence of reduced regeneration of ADP and $NADP^+$ due to some metabolic impairment or nutrient deficiency. Therefore, an efficient ability to regulate the energetic fluxes along the photosynthetic electron transport chain is a crucial requisite for the fitness of photosynthetic organisms. As a result, photosynthetic organisms need to constantly regulate the mechanisms of light capturing and utilization, to maintain sufficient photochemical activity but avoiding photodamage (Erickson et al., 2015).

Evolution provides photosynthetic organisms with mechanisms to protect photosystems and preserve their functionality. Among these, the most responsive is the non-photochemical quenching (NPQ) of Chls, that rapidly dissipates the excess energy absorbed as heat, preventing triplet states formation (Horton, 1996). NPQ response is triggered through a feedback mechanism by thylakoid lumen acidification, which is caused by saturation of the photosynthetic electron transport chain (Genty et al., 1989). Because evolution aims to

guarantee plant survival, and not an optimized productivity, understanding the molecular mechanism of NPQ activation and deactivation process have a great biotechnological relevance to improve the fitness and yield of photosynthetic organisms (Kromdijk et al., 2016; Głowacka et al., 2018). Microalgae raised interest for biotechnological applications, being photosynthetic microorganisms which can be cultivated in industrial environment as biofactories for bioproducts of interest, like food additives, nutraceuticals, antioxidants, biostimulants, and even biofuels (Medipally et al., 2015; Bernaerts et al., 2019; Camacho et al., 2019; Koyande et al., 2019; Rani et al., 2021). In the model organism for green algae, *Chlamydomonas reinhardtii,* the key proteins responsible for this mechanism activation are the pigment binding proteins LHCSR1 (Light Harvesting Complex Stress Related 1) and LHCSR3 subunits, with the latter having a predominant role (Peers et al., 2009). Expression of LHCSRs is strongly induced upon high light exposure. LHCSR proteins were reported to sense lumen acidification upon protonation of specific exposed residues, thus being able to switch from a light-harvesting state to a quenched one triggering NPQ (Peers et al., 2009; Liguori et al., 2013; Ballottari et al., 2016; Troiano et al., 2021).

While LHCSR is the trigger, it needs to interact with other antenna proteins of the photosystems to efficiently induce NPQ (Tokutsu and Minagawa, 2013; Dinc et al., 2016). In *C. reinhardtii*, PSII light antenna are organized in two different moieties: trimeric major light-harvesting complexes (LHCII) and monomeric subunits (Shen et al., 2019). Trimeric LHCII are encoded by nine genes called *lhcbm1–lhcbm9* (with M referring to 'major' antenna complex) (Minagawa and Takahashi, 2004; Drop et al., 2014). Conversely, CP26 and CP29 are the two the monomeric LHC subunits which have a key role as linker between the RC and the external LHCII (Drop et al., 2014; Semchonok et al., 2017; Cazzaniga et al., 2020). Indeed *C. reinhardtii* PSII homodimer RC is surrounded by two antenna layers (Tokutsu et al., 2012): the inner layer is composed of CP29, CP26, and S-LHCII (S, strongly bound), forming with the core the C_2S_2 particle, whereas the outer layer is made of M-LHCIIs (moderately bound) forming with C_2S_2, the $C_2S_2M_2$ supercomplex. An additional LHCII (N-LHCII) can be connected directly to the PSII core in the position that in vascular plants is occupied by the third monomeric antenna CP24 (absent in *C. reinhardtii*), forming the larger $C_2S_2M_2N_2$ (Drop et al., 2014). The presence of these additional trimer depends on the light regime at which the microalgae are adapted: in low/limiting light conditions the photosystems increase the amount of LHCII to try to capture all the disposable light while in high light the LHCII per core complex decrease to avoid excess light absorption and photodamage.

The different LHC subunits have similar biochemical and biophysical properties (Natali and Croce, 2015), but despite these structural similarities, different antennas have been suggested to have different roles in the light harvesting mechanism and photoprotection. Indeed, the NPQ phenotype of specific *lhcbm* knock out or knock down mutant led to the suggestion of peculiar roles in NPQ for LHCBM1 and LHCBM4-6-8. In the case of monomeric antenna LHC subunits, we recently reported a strong reduction of light harvesting and NPQ mechanisms in a *C. reinhardtii* mutant deprived of both CP26 and CP29 (Cazzaniga et al., 2020), consistently with previous work, suggesting LHCII and CP26 as docking sites for LHCSR3 upon NPQ induction in *C. reinhardtii* (Semchonok et al., 2017). In this study, we further characterize the role of

monomeric antenna subunits using CRISPR/Cas9 genome editing and complementation of CP26 gene in *C. reinhardtii*. *cp26* mutant (herein named *k6*) showed partially reduced photosynthetic efficiency, reduced growth compared to its parental strain, and a strong impairment in NPQ induction. According to our data, we propose CP26 as a crucial interactor with LHCSR protein, essential for NPQ activation, while both CP26 and CP29 are key proteins for light harvesting and energy transfer to RC.

RESULTS

Generation of CP26 deficient Chlamydomonas mutant

To investigate the role of CP26 in *C. reinhardtii*, a reverse genetic approach was applied to knock out the CP26 gene (lhcb5, Cre16.g673650) through CRISPR/Cas9-mediated gene disruption (Baek et al., 2016; Kim et al., 2020) (Figure 1). The mutants were generated in the CC-503 cell wall-deficient strain, here referred to as wild-type (Wt) (Hyams and Davies, 1972). The sgRNA target located in exon 4 yielded successful results, leading to non-homologous end joining and Cas9-mediated hygromycin-resistance (HygR; aphVII) gene cassette insertion in the target site (Figure 1a). The genomic sequence of knock-out mutants (CP26 gene) revealed that the gRNA binding site of CP26 was mutated. Insertion of HygR gene cassette in the coding DNA sequence (CDS) of the target gene was confirmed by PCR and Sanger sequencing (Figure1b, c, and Figure S1a, and Table S1) and the lines were named *k6#1-11*. Ten mutants were validated by immunoblot analysis with a specific antibody against CP26 confirming the absence of the protein (Figure 1d, Figure S1b). Southern blot analysis on the selected lines showed that *k6#4* and *k6#8* contained a single insertion of the HygR gene in the genome, while the others displayed multiple insertions (Figure S1c). These two mutants were considered for subsequent analysis; *k6* data in the following parts of experiments are presented as the average of these two lines. Moreover, the separation of isolated thylakoid membrane polypeptides from Wt and *k6* revealed that the *k6* mutant lacks the band corresponding to CP26 (Figure 1e).

Pigment content and Pigment-Protein Complexes stoichiometry in the mutant without CP26

Pigment content was analyzed in Wt and *k6* cell cultures, grown in Tris-acetate phosphate (TAP) (Kropat et al., 2011) at 80-100 μmol m^{-2} s^{-1} for at least three generations (Table 1). The mutant, compared to its parental line, displayed a similar Chl content per cell, but a slightly lower Chl a/b ratio. The Chl per car ratio and the Car composition were comparable between the two genotypes, as confirmed by the high-performance liquid chromatography (HPLC) analysis showing only minor and not significant differences in loroxanthin and antheraxanthin content. At this light intensity, zeaxanthin accumulation was not detected.

A partial rearrangement of the photosynthetic complexes in *k6* lines could account for a lower Chl a/b ratio, being Chl b only bound by antenna subunits while Chl a is present in all pigment-binding complexes. To assess this hypothesis, we measured the relative amounts of PSI, PSII, LHCII and CP29 using specific antibodies against the different photosynthetic subunits (Figure 2). In particular, CP43 and PsaA were used as proxies for PSI and PSII content, respectively, while LHCII content was investigated using an antibody

recognizing the different LHCBM subunits of *C. reinhardtii,* revealing the presence of three main bands: the upper one corresponding to *lhcbm3-6* and *lhcbm8* gene products, the one in the middle to *lhcbm1* and the lower one to *lhcbm2* and *lhcbm7* (Girolomoni et al., 2017). Compared to Wt, the *k6* mutant showed increased PSI/PSII and LHCII/PSII ratios where LHCII content per PSII was almost doubled, suggesting an internal compensation of the absence of monomeric antenna by an increase of the LHCII protein level. The increased LHCII content was related to an increased accumulation of all the different LHCBM subunits detected (Figure 2a). In the case of CP29, the CP29/PSII ratio was similar in *k6* compared to the Wt case. The organization of pigment binding complexes was further analysed by Non-denaturing Deriphat-PAGE, upon solubilisation of thylakoid membranes with dodecyl-α-D-maltoside (α-DM) (Figure 2c). Different pigment binding bands were resolved, corresponding from bottom to top respectively to free pigments (1), LHC antenna in monomeric state (2), trimeric LHCII (3), PSII core complex (4) and PSI-LHCI (5-6). The densitometry of these bands confirmed the data from the immunotitration analysis: *k6* mutant showed a relative increase of the bands corresponding to antenna proteins (2, 3) and to PSI (5-6) compared to PSII core (4). It is important to note that the reduced Chl a/b ratio and the increased PSI/PSII and LHCII/PSII ratios observed in *k6* are essentially in line with previous observations in the *C. reinhardtii* mutant *k9*, where CP29 was absent, while in the double mutant *k69* the LHCII and PSI per PSII content were further increased (Cazzaniga et al., 2020). However, it is important to point out that while the CP29/PSII was similar in *k6* and Wt, in the case of *k9* mutant a ~50% increase in CP26/PSII ratio compared to the Wt case was observed (Figure S2), likely to partially compensate for the absence of CP29.

Light harvesting efficiency

The consequences of CP26 absence on the activity of PSII were initially evaluated by measuring PSII maximum quantum efficiency (F_v/F_m) in dark-adapted cells (Butler, 1973), revealing a significant decrease in the mutant (0.67 vs 0.72 in *k6* and Wt, respectively) (Table 1). Such difference is attributable to a higher basal fluorescence (F_0) in the mutant when exposed to weak measuring light, as reported by the fluorescence values normalized to the Chl amount (Figure S3). Being F_0 measured in limiting light condition, a higher F_0 value in the *k6* indicates that a fraction of the absorbed light energy is not efficiently directed toward photochemistry but re-emitted as fluorescence; indeed, the lack of the monomeric antenna CP26 could alter the connection between the antenna complex, somehow impairing the energy transfer from LHCII to RC. This alteration can be observed also by measuring fluorescence emission spectra at 77K (Figure 3a): *k6* cells were characterized by an additional shoulder at ~680 nm, usually assigned to "disconnected" LHC complexes, meaning LHC proteins are impaired in energy transfer to Photosystems, thus re-emitting fluorescence at shorter wavelengths (Garnier et al., 1986). *k6* mutant was thus characterized by an increased LHCII content, which however are partially not able to transfer energy to PSII: a similar phenotype could be observed in absence of CP29 (*k9* mutant) or, to a higher extent, in the double *k69* mutant, without both CP26 and CP29, (Figure S4a) consistently with previous data (Cazzaniga et al., 2020). The light harvesting capacity of PSII, or functional PSII antenna size, was thus evaluated from the kinetics of Chl a fluorescence induction in whole cells in limiting light conditions, upon treatment with PSII inhibitor DCMU: in this

condition the rise time of chlorophyll fluorescence is inversely proportional to PSII light harvesting feature (Malkin et al., 1981). *k6* showed a functional antenna size similar to the Wt case, even with a doubled LHCII/PSII ratio, further suggesting a reduced antenna-to-core energy transfer efficiency in this mutant (Figure 3b). Energy transfer to PSII RC was thus investigated on whole cells by measuring time-resolved fluorescence decay on Wt and *k6* cells using 475-nm excitation (Figure 3c). In absence of CP26, the fluorescence decay traces were slower compared to the Wt case. Similar results could be obtained in the case of *k9* and *k69* (Figure S4b). As reported in Table S2, fitting analysis with exponential functions allow to estimate the average lifetimes of fluorescence decay, which were increased in *k6, k9* and *k69* compared to Wt, with the longest lifetime in the double mutant. These results confirm that in absence of CP26 energy transfer from LHCII to RC was partially impaired, with a more evident consequences when both CP26 and CP29 were absent.

PSII photochemical activity was then investigated in *k6* and its parental strain by measuring PSII operating efficiency (ΦPSII), PSII electron transport rate (ETR) and photochemical quenching (1-qL) at different light intensities (Baker, 2008). As reported in Figure 4, these photosynthetic parameters were not significantly different between the Wt and *k6* mutant. The only exception is represented by the ΦPSII at low light intensities, that showed lower values in the *k6* mutant. These results are different compared to the *k9* and *k69* case, where a strong reduction in ETR and ΦPSII was observed, especially in the double *k69* mutant (Figure S4), consistent with previous findings (Cazzaniga et al., 2020). The influence of CP26 on light dependent oxygen production was then investigated at different actinic lights (Figure 4d). Despite having a similar maximum light dependent oxygen production rate (Pmax), *k6* mutant was characterized by a reduced oxygen production at low and intermediate irradiances (Figure 4d, Table S3). The respiration in the dark was not affect by CP26 absence. However, a more evident decrease in oxygen production could be observed in the absence of CP29 in *k9* mutant and even further in the double mutant *k69*. From these data, the *k6* showed a lower photochemical efficiency compared to Wt only at low-medium light, while a more severe reduction of PSII activity, even at high irradiances, could be observed in the absence of CP29 or both CP26 and CP29 (Figure S4).

Biomass productivity

To evaluate how these defects in *k6* could affect biomass yield, growth curves of both Wt and *k6* strains were monitored in photoautotrophy at low (40 μmol m^{-2} s^{-1}), medium (80-100 μmol m^{-2} s^{-1}) and high light (700-800 μmol m^{-2} s^{-1}) (Figure 5). Under low or medium irradiances, the absence of CP26 caused a significant delay in growth rate reaching in the case of *k6* mutant a cell density around half of the Wt. However, in the absence of CP29 (*k9* mutant) or both CP26 and CP29 (*k69* mutant) a much stronger reduction in biomass productivity could be observed (Figure S5). At higher light intensities, where light is not limiting, the growth curves of Wt, *k6, k9* and *k69* strains were similar (Figure 5c, Figure S5).

Non Photochemical Quenching induction

Previous work demonstrated that the photoprotective induction of NPQ was essentially impaired in the absence of CP26 and CP29, but still active in the absence of CP29 only (Cazzaniga et al., 2020). The availability of a single *k6* mutant depleted of CP26 allows to investigate the specific function of this LHC complex in NPQ induction in *C. reinhardtii*. Because LHCSR proteins are required to induce NPQ (Peers et al., 2009), Wt and *k6* strains were exposed to high light (1200 µmol m^{-2} s^{-1}) for two days to induce LHCSR1 and LHCSR3 (Allorent et al., 2013). LHCSR proteins accumulation was investigated by immunoblotting (Figure S6), revealing an increased content per PSII of both LHCSR1 and LHCSR3 in *k6* compared to Wt: LHCSR1/PSII ratio was increased by ~48% and LHCSR3/PSII by ~70% in *k6* compared to the Wt case. NPQ induction at different actinic lights was thus investigated (Figure 6): dark adapted cells were illuminated for fifteen minutes followed by dark relaxation. Upon exposure to an actinic light of 1200 µmol photons m^{-2} s^{-1}, NPQ in the Wt reached a final value of ~2.5, fully recovering after 3 minutes of relaxation in the dark, while maximum NPQ value in the *k6* mutant was ~0.7 (Figure 6a). As reported in Figure 6b the maximum NPQ induced by *k6* mutant at different actinic light was always strongly reduced compared to the Wt case with a residual NPQ ranging from ~6% at 150 µmol photons m^{-2} s^{-1} and ~30% at 2400 µmol photons m^{-2} s^{-1} in the mutant (Figure S7). In the case of *k69* double mutant, the NPQ was further reduced (Figure S8), with a residual NPQ compared to Wt ranging from 0% at 150 µmol photons m^{-2} s^{-1} to 10% at 2400 µmol photons m^{-2} s^{-1}, consistently with previous findings (Cazzaniga et al., 2020). The absence of CP29 instead had a minor effect on NPQ with a residual NPQ compared to the Wt case ranging from 50% at 150 µmol photons m^{-2} s^{-1} to 90% at 2400 µmol photons m^{-2} s^{-1}.

NPQ is triggered by thylakoid lumen acidification. The NPQ phenotype observed in *k6* mutant could in principle be related to a reduced capacity in the mutant to generate a proton gradient across the thylakoid membrane upon illumination. To overcome this possible bias, light independent NPQ activation was induced by direct lumen acidification adding acid solution to the cells as previously reported (Tian et al., 2019). To validate the procedure, we first tested direct acidification on null NPQ mutant (*npq4 lhcsr1,* lacking both LHCSR1 and 3) and its parental strain (4a+) (Figure S9). Cells were first adapted to high light for two days to induce LHCSR and then maximum fluorescence emissions were measured applying saturating pulses, before (F_m) and after (F_m^a) decreasing the pH with acid solution. In 4a+ the F_m^a is lower than the F_m with a calculated NPQ value of ~1.93 while the *npq4 lhcsr1* mutant displayed identical values of the two parameters and a null NPQ, thus confirming the reliability of the procedure. The same measurements were then repeated on Wt and *k6* strains (Figure 7). In the Wt, the acidification induced a strong decrease of F_m^a compared to F_m with a calculated NPQ of 1.76, whereas in *k6*, the same procedure induced only a limited decrease of the F_m^a and a NPQ of 0.52. These differences between Wt and *k6* are comparable to the ones obtained inducing NPQ by light exposure, further suggesting that the impaired quenching in *k6* is mainly caused by a hampered NPQ mechanism rather than an impairment in the thylakoid lumen acidification. The same approach tested on *k9* and *k69* cells showed that the mutant without CP29 had a level of NPQ similar to Wt while the double mutant *k69* showed a strongly reduced level of quenching (Figure S10).

Rescue of NPQ phenotype by genetic complementation

NPQ reduction was the main phenotype observed in *k6* mutant compared to Wt. Therefore, a genetic complementation approach was performed to correlate this phenotype adequately with the absence of CP26. First, we tried to use the whole CP26 genomic sequence including, native promoter, 5'-UTR, 3'-UTR and terminator (Figure S11). However, we were unable to synthetize or amplify the 1000 bp upstream the CDS, due to its complexity and to the presence of an un-sequenced region into the genome. To overcome this issue, we decided to exploit the 1000 bp upstream region of the other monomeric antenna CP29 (Cre17.g720250) as putative promoter, which did not pose the same challenge as the CP26 region. This chimeric construct (CP29, 1000 bp upstream- CP26 gene from 5'UTR to 3'UTR- CP26, 300 bp downstream) was then introduced in the *k6#8* mutant line, resulting in the successful accumulation of CP26 protein. The CP26 expressing lines in *k6* background, herein named as *k6c* (*k6* complemented), were analyzed by western blot analysis. Different levels of CP26 expression were observed in *k6c* lines, ranging from ~10% to 200% of the Wt CP26/PSII ratio (Figure S12). *k6*c lines were adapted for two days in high light and the NPQ was measured as described previously upon exposure to 1200 µmol photons m^{-2} s^{-1} actinic light. As seen in Figure 8a, in the case of five different complemented lines displaying a CP26/PSII ratio comparable to Wt (Figure S12), the NPQ induction kinetics were similar between Wt and the selected *k6c* lines, highlighting that the NPQ phenotype in *k6* was specifically due to the absence of CP26. Moreover, in these lines the Fv/Fm values were similar to that in Wt, confirming the correlation between the lack of CP26 expression and decreased PSII efficiency (Figure S12). NPQ values obtained for the different complemented lines expressing different levels of CP26 were then plotted as a function of CP26/PSII ratio (Figure 8b). The correlation between NPQ level and CP26/PSII ratio can be divided into two phases: in the first phase NPQ values increase proportionally with the CP26/PSII ratios. When CP26 content per PSII was at least 50% of that of Wt, the NPQ induction capability was saturated and similar to that in Wt, despite a further increase in CP26/PSII ratio up to 200% compared to Wt. These data confirm the crucial role of CP26 in the mechanism underlying NPQ in *C. reinhardtii*, indicating that half of the CP26/PSII content observed in Wt is sufficient to ensure the complete activation of this photoprotective mechanism.

DISCUSSION

In a previous study, we analyzed the effect of the absence of CP29 or both CP26 and CP29 in *C. reinhardtii* (Cazzaniga et al., 2020). The simultaneous absence of CP26 and CP29 impaired both photosynthetic efficiency and photoprotection with an almost complete impairment of NPQ induction (Cazzaniga et al., 2020); these results were further confirmed in this study (Figure S8). However, a comprehensive study of the specific role of CP26 protein in light harvesting and NPQ mechanism of *C. reinhardtii* still lacked so far. The CRISPR/CAS9 approach attempted in our previous work to obtain a single *cp26* mutant indeed resulted in the absence of both CP26 and CP29 (Cazzaniga et al., 2020). In this study we successfully generated a single *k6* mutant by selecting new target regions for CAS9 activity which did not affect CP29 expression

285 (Table S1). On the base of our findings we can thus suggest that the absence of CP29 in the lines generated
286 by CRISPR/CAS9 targeted to *CP26* gene in our previous work (Cazzaniga et al., 2020) was likely related to
287 some off-target mutations induced by CAS9 at the level of *CP29* gene or to some other genes which control
288 the expression of CP29 at translational or post-translational level. These mutations are, however, extremely
289 difficult to be detected and properly evaluated. Here, the availability of a single *k6* mutant and its
290 complemented lines allow to investigate the effects of the lack of this monomeric antenna on photosynthesis
291 and cell physiology.

292 In the absence of CP26, Fv/Fm was lower, due to an increase of the F_0 fluorescence, and the low temperature
293 fluorescence showed a shoulder around 680 nm that represent defectively connected LHCII (Figure 3).
294 Similar results were obtained in the absence of CP29 and were even more evident in the double mutant *k69*
295 (Figure S4a). These data imply a reorganization of PSII supercomplex in the absence of monomeric antenna
296 subunits, with a reduced efficiency of energy transfer from a portion of the antenna system to the core.
297 Accordingly, time-resolved fluorescence analysis on whole cells demonstrated a reduced energy transfer
298 from PSII antenna complexes to the RC in the absence of CP26, CP29 or both (Figure 3c, Figure S4b).
299 Moreover, in *k6* the LHCII content was strongly increased compared to Wt (Figure 2) similarly to previous
300 result on the single *k9* mutant, but less evident compared to the double *k69* mutant strains (Cazzaniga et al.,
301 2020). It is important to note that CP29 subunit stoichiometry per PSII was not changed in *k6*, while *k9*
302 mutant partially compensate the absence of CP29 by a 50% increase of CP26 (Figure S2). Detailed electron
303 microscopy analysis would be required to assess if the extra CP26 produced in *k9* mutant partially substitute
304 CP29 in PSII supercomplexes. These results indicate the possibility of a compensatory mechanism that
305 increases the amount of antenna to counteract a less efficient excitation energy transfer to PSII RC. This
306 compensatory increase in LHCII was not entirely successful for all mutant strains, as can be seen by
307 appearance of fluorescence signatures at 77K related to "unconnected" LHCII in the absence of CP26, CP29
308 or both. Moreover, in *k6* the functional antenna size was similar to the Wt even if the amount of LHCII was
309 almost doubled (Figure 3). The reduced energy transfer efficiency in the absence of CP26 influenced the
310 photosynthetic activity of PSII, causing reduced light dependent oxygen evolution, especially at low-medium
311 irradiances (Figure 4, Table S3). However, the similar Pmax of Wt and *k6* mutant suggest that proper PSII
312 photochemical activity can be restored even in the absence of CP26, providing increased photons to
313 counterbalance the reduced light harvesting efficiency observed in the mutant. These results differ from that
314 of the mutant strains without CP29 (*k9* and *k69*), where the oxygen evolution rates were always lower than
315 that in the Wt, resulting in reduced Pmax, consistent with previous results. The altered photosynthetic
316 activity in absence of CP26 also affected biomass accumulation; when grown in limiting light condition, the
317 *k6* exhibited a lower cellular density, and the growth rate was reduced. However, a more severe reduction in
318 growth rate could be observed in the case of *k9* and *k69*, consistent with the lower photosynthetic activity
319 measured in the absence of CP29 or both CP26 and CP29 compared to the case where only CP26 is missing.
320 When mutant strains were grown at higher light intensities (700-800 μmol m^{-2} s^{-1}) similar growth curves
321 were observed for Wt and mutant strains, suggesting that in these conditions light harvesting and PSII

activity was not limiting the growth. All these data point out that the absence of CP26 reduces light harvesting efficiency of the cells and it is relevant in low light conditions. The comparison of *k6*, *k9* and *k69* highlights that both monomeric antenna proteins are important for efficient light harvesting in *C. reinhardtii* but CP29 have a prominent role. These functional differences correlate with the position of the two antennae in the PSII supercomplex. CP29 is located in the inner layer of the antenna and interact with trimers S-LHCII, M-LHCII and marginally with additional N-LHCII while CP26 is in a more external position and interact only with S-LHCII that is still connected to the RC from the other side through CP29 (Shen et al., 2019). Due to this organization, the absence of CP29 had a stronger impact on PSII antenna complex and on efficiency of light energy direction toward the core complex.

Photosynthetic organisms evolved specific strategies to maximize light harvesting in low light condition and avoid excess energy absorption in high light. In the case of the model organism for green algae, *C. reinhardtii*, NPQ induction requires the presence of LHCSR proteins which upon thylakoid lumen acidification, are activated through their pH sensing residues (Liguori et al., 2013; Ballottari et al., 2016). Activation of LHCSR subunits switch their conformation from a light harvesting to a dissipative state being able to quench the excitation energy from PSII complex (Tokutsu and Minagawa, 2013; Liguori et al., 2016). LHCSR proteins need to interact with other antenna proteins to efficiently redirect and quench the excess light energy absorbed. (Liguori et al., 2013; Ballottari et al., 2016). Alternatively, it cannot be excluded that LHCSR can trigger a conformational change in other antenna subunits, leading to the formation of additional energy dissipation sites (Tokutsu and Minagawa, 2013). Previous works demonstrated by electron microscopy the interaction of LHCSR3 dimers with CP26 and LHCII subunits but the specific functions of the different antenna proteins in the NPQ process has not been fully elucidated yet. In the case of LHCII, the absence of LHCBM1 (Elrad et al., 2002) or downregulation of LHCBM4-6-8 subunits (Girolomoni et al., 2017) caused a reduction of NPQ induction, suggesting these subunits as potential partners for LHCSR3. Our previous findings demonstrated that in the absence of monomeric CP26 and CP29 subunits, NPQ induction was essentially impaired in *C. reinhardtii* (Cazzaniga et al., 2020).

Here we can narrow down our knowledge, demonstrating a specific function for CP26. The NPQ was strongly reduced in *k6* mutant at all the light intensities tested, even with strong actinic light (Figure 6, Figure S7). The absence of CP29 in *k9* also caused a decrease in NPQ compared to Wt but to a lesser extent compared to that in *k6*. While a more dramatic NPQ phenotype was observed in the absence of both CP26 and CP29 subunits in *k69* (Figure S8). The impaired NPQ mechanism in *k6* could be due to a decreased LHCSR/LHCII ratio which was reduced in *k6* compared to that in Wt. The relatively reduced LHCSR/LHCII stoichiometry in *k6* could indicate a lower possibility to quench the increased amount of trimer in the absence of CP26 resulting in a lower level of NPQ. However, in the *k9* the LHCSR/LHCII ratio was similar to that in *k6* (Cazzaniga et al., 2020) but the NPQ induction was less affected. Thus, reduced NPQ in the absence of CP26 may not be due to the alteration of LHCSR/LHCII ratio. Different lumen acidification could also be excluded as possible explanation for reduced NPQ observed in *k6*, according to the similar NPQ impairment observed upon induction of NPQ in the dark by artificial lumen acidification, by-passing

any eventual effect due to impairment in light energy transfer to the electron transfer chain. The specific role of CP26 in NPQ was confirmed by the genetic complementation of *k6* mutant (Figure 8). Moreover, the obtained complemented lines, displaying different amounts of CP26 antenna protein, allowed us to study the correlation between CP26/PSII ratios and NPQ mechanism. Interestingly, accumulation of CP26 per PSII to a 50% level compared to that in Wt was sufficient to fully restore NPQ. PSII supercomplexes are included in the tightly stacked grana of the thylakoid membranes and single PSII can pair up with near complexes or connect with complexes across the stromal gap (Albanese et al., 2017). It is possible to speculate that these close interactions may allow CP26 to interact with different complexes, reducing the amount needed of this subunit to transfer excitation energy from PSII to the quenchers, as LHCSR proteins. These data confirm the fundamental importance of monomeric antenna subunits in the quenching mechanism (Cazzaniga et al., 2020) but indicate CP26 as the monomeric antenna protein with a prevalent role in NPQ. These results are consistent with previous evidence that points out to CP26 as docking sites for LHCSR3 on PSII supercomplexes (Kim et al., 2017; Semchonok et al., 2017). LHCSR proteins are not constitutively expressed in *C. reinhardtii* but only upon high light exposure stress (Tokutsu and Minagawa, 2013): being in an external position, CP26 could represent a more accessible point for a direct interaction with LHCSR3, while CP29 is clamped between the core and S- and M-LHCII (Drop et al., 2014; Cao et al., 2020). Monomeric CP26 could thus be essential for the energy transfer from the antenna complex to LHCSR subunit. The dramatic difference in NPQ between *k6* and *k9* could be influenced also by the change of expression level of the remaining monomeric antenna in the single mutants. While in Wt and *k6* the relative amount of CP29 is similar, *k9* shows an over-accumulation of CP26 protein, with an increase of ~ 50 % with respect to Wt. This increase in CP26 could partially compensate for the absence of CP29. This implies that CP26 could interact also with PSII core in the region where normally CP29 resides improving LHCII connection. This compensatory mechanism has never been observed in *Arabidopsis thaliana,* where CP29 binding site cannot be occupied by other subunits (de Bianchi et al., 2011). In *A. thaliana,* where the absence of CP26 had no effect on the quenching mechanism, the simultaneous deletion of all monomeric subunits reduced the light harvesting capacity but had a minor role in NPQ (de Bianchi et al., 2008; Dall'Osto et al., 2020). The data from this study further confirm the differences between LHCSR-dependent NPQ observed in *C. reinhardtii* and the well-known PSBS-dependent NPQ in vascular plants. In both cases, LHCSR proteins and PSBS need to interact with LHC proteins to trigger NPQ (Niyogi and Truong, 2013; Sacharz et al., 2017): a possible different affinity of LHCSR and PSBS for the specific LHC antenna could explain the different phenotype observed in LHC mutant in *C. reinhardtii* compared to *A. thaliana*.

In conclusion, these results point out a distinct role of the two monomeric antenna subunits in *C. reinhardtii*. Both are important for light absorption and photoprotection with the more evident phenotypes observed in the double mutant *k69,* where both CP26 and CP29 are absent. While CP29 is fundamental for efficient light harvesting and PSII activity, CP26 plays a major role in NPQ induction. It is important to note that a small induction at very high light could still be observed in the absence of both CP26 and CP29: this residual NPQ was probably due to the interaction of LHCSR1 or LHCSR3 with LHCII subunits, as previously reported

(Kim et al., 2017; Semchonok et al., 2017). These data could be useful to further understand the NPQ in microalgae and to identify target to tune this mechanism to increase microalgal productivity under different light regimes.

MATERIALS AND METHODS

Generation of C. reinhardtii mutants by CRISPR-Cas9 genome editing

To generate knock-out CP26 mutants, CRISPR-Cas9 RNP complex-mediated genome editing method was performed according to (Kim et al., 2020) and (Joo et al., 2022) with a few modifications. The sgRNA sequence for the CP26 mutant generation using CRISPR-Cas9 was designed by Cas-Designer (http://www.rgenome.net/cas-designer) and selected as 5′- CCCGAGGGCCTGCAGGCCAACGG -3′ (Figure 1a). To increase the efficiency and fast selection of CP26 mutants, insertion and expression of hygromycin-resistance (HygR; aphVII) gene cassette was combined. 100 µg of purified Cas9 protein (Cas9 expression plasmid: pET-NLS-Cas9-6xHis (Plasmid #62934)) and 70 µg of sgRNA synthesized by using GeneArt™ Precision gRNA Synthesis Kit (ThermoFisher, MA, USA), were mixed to form the RNP complex and co-transformed with aphVII gene expression cassette. After transformation, cells were plated on TAP medium containing 1.5% agar and hygromycin (25 µg/ml). To screen CP26 knock-out mutants, the colonies grown onto the selection plate were confirmed by genomic PCR using the target-specific primer set (forward: 5′- CTTTCAGTCAGCTTGCATGG -3′, reverse: 5′-AGGGGGTTGGACACAATG -3′). The PCR products were sequenced using Sanger sequencing by Macrogen Inc. (Seoul, South Korea). To verify the integration and copy number of the aphVII gene in the genome, the genomic DNA was digested by *Kpn*I or *Nco*I, and Southern blot analysis was performed using aphVII gene probe for detection of DNA integration. Bands were visualized using the Gene Images AlkPhos Direct Labeling and Detection System (Amersham, Little Chalfont, Bucks, United Kingdom).

Culture conditions

C. reinhardtii Wt (CC503) and mutant strains were grown at 24°C in high-salts (HS) medium (Kropat et al., 2011) on a rotary shaker in Erlenmeyer flasks under continuous illumination with white LED. Cell densities were measured using Countess II FL Automated Cell Counter (Thermo Fisher Scientific).

Membrane preparation, Gel electrophoresis and immunoblotting

Thylakoid membranes were isolated as previously described (Bonente et al., 2008). SDS-PAGE analysis was performed using the Tris-Tricine buffer system (Schägger and von Jagow, 1987) followed by Coomassie blue staining. For immunotitration, thylakoid samples were loaded for each sample and electroblotted on nitrocellulose membranes; then, proteins were quantified with an alkaline phosphatase–conjugated antibody system. αCP26 (AS09 407), αCP29 (AS04 045), αLHCII (AS01 003) αCP43 (AS11 1787), αPSAA (AS06 172), αLHCSR1 (AS14 2819), αLHCSR3 (AS14 2766) antibodies were purchased from Agrisera (Sweden). Non-denaturing Deriphat-PAGE was performed following the method developed in (Peter et al., 1991).

Thylakoids concentrated at 1 mg/ml Chls were solubilized with a final 0.8% α-DM, and 30 µg of Chls were loaded in each lane.

Pigment and spectroscopy analysis

Pigments were extracted from intact cells using 80% acetone buffered with Na_2CO_3 and analyzed by reverse-phase HPLC (Lagarde et al., 2000). HPLC system (HPLC Jasco Extrema LC-4000) equipped with a C18 column (Synergy Hydro-RP, Phenomenex) using a 15-min gradient of ethyl acetate (0%–100%) in acetonitrile–water–triethylamine (9:1:0.01) at a flow rate of 1.5 mL/min was used (Perozeni et al., 2020). Pigment detection was conducted with a 350–750 nm diode array. 77 K fluorescence emission spectra on frozen cell were registered using a BeamBio custom device equipped with USB2000 Ocean Optics spectrometer (Ocean Optics).

Time-resolved fluorescence on whole cells

Time-resolved fluorescence measurements were carried out using a Ti: sapphire laser (Chameleon Ultra II, Coherent, repetition rate of 80 MHz and 140 fs pulse width). A β-barium borate (BBO) crystal was used to frequency double the 950 nm laser output in order to generate the 475 nm excitation wavelength. The fluorescence signal from the cells was focused on the entrance slit of a spectrograph (Acton SP2300i, Princeton Instrument). A streak camera (C5680, Hamamatsu), equipped with the Synchroscan sweep module, which provides spectral-temporal matrices with spectral and temporal resolutions of ∼1 nm and ∼20 ps, respectively, for the temporal window of 2 ns. A CCD (Hamamatsu ORCA-R2 C10600) recorded the streak image. The measurements were carried out in cuvettes with optical path-length of 10 mm and the sample was under constant circulation from a reservoir of 30 mL sample volume through a tube and peristaltic pump to avoid any photodamage of the samples.

Measurements of photosynthetic activity

Photosynthetic parameters ΦPSII, qL, electron transport rate (ETR), and NPQ were obtained by measuring with a DUAL-PAM-100 fluorimeter (Heinz–Walz) chlorophyll fluorescence of intact cells, at room temperature in a 1 × 1-cm cuvette mixed by magnetic stirring. ΦPSII, qL, and ETR were measured and calculated according to (Baker, 2008) and (Van Kooten and Snel, 1990) at steady-state photosynthesis upon 20 min of illumination. NPQ measurements were performed on dark-adapted intact cells as described in (Cazzaniga et al., 2020) with the following modifications: cells were adapted to high light only for two days before NPQ measurements and far-red light exposure was performed for 2 minutes before turning on the actinic light. PSII functional antenna size was measured from fast chlorophyll induction kinetics induced with a red light of 11-µmol photons m^{-2} s^{-1} on dark-adapted cells (~$2 \cdot 10^6$ cells/ml) incubated with 50-µM DCMU. The reciprocal of time corresponding to two thirds of the fluorescence rise (τ2/3) was taken as a measure of the PSII functional antenna size (Malkin et al., 1981). The oxygen evolution activity of the cultures was measured at 25°C with a Clark-type O2 electrode (Hansatech), as described previously (Cazzaniga et al., 2020).

Acid induced quenching

NPQ acid induction in the dark was induced as previously described (Tian et al., 2019): in brief, cells were centrifuged (3 min, 1000 g), resuspended in water at the density of 10^6 cells/ml and were acidified by adding 5 mM acetic acid. Fluorescence was measured with a PAM-101 fluorimeter (Walz, Effeltrich, Germany) and NPQ was calculated upon reaching steady state fluorescence levels.

k6 mutant complementation

Vector used for knockout complementation was obtained by fusion PCR merging the 1000bp upstream 5'UTR of CP29 gene (Cre17.g720250) with the whole CP26 gene (Cre16.g673650) deprived of promoter region and extended of 300bp downstream 3'UTR. This sequence was cloned into pOpt2 vector system and used for transformation. Nuclear transformation was carried out by glass bead as previously described (Perozeni et al., 2020) using 10 µg of linearized plasmid followed by selection of transformants on TAP agar plates (Kropat et al., 2011) supplied by paromomycin (10 mg/L) for 6–7 days.

REFERENCES

Albanese P, Melero R, Engel BD, Grinzato A, Berto P, Manfredi M, Chiodoni A, Vargas J, Sorzano CÓS, Marengo E, Saracco G, Zanotti G, Carazo J-M, Pagliano C (2017) Pea PSII-LHCII supercomplexes form pairs by making connections across the stromal gap. Scientific Reports **7:** 10067

Allorent G, Tokutsu R, Roach T, Peers G, Cardol P, Girard-Bascou J, Seigneurin-Berny D, Petroutsos D, Kuntz M, Breyton C, Franck F, Wollman FA, Niyogi KK, Krieger-Liszkay A, Minagawa J, Finazzi G (2013) A dual strategy to cope with high light in Chlamydomonas reinhardtii. Plant Cell **25:** 545-557

Aro E-M, Virgin I, Andersson B (1993) Photoinhibition of Photosystem II - inactivation, protein damage and turnover. Biochim.Biophys.Acta **1143:** 113-134

Baek K, Kim DH, Jeong J, Sim SJ, Melis A, Kim JS, Jin E, Bae S (2016) DNA-free two-gene knockout in Chlamydomonas reinhardtii via CRISPR-Cas9 ribonucleoproteins. Sci Rep **6:** 30620

Baker NR (2008) Chlorophyll fluorescence: a probe of photosynthesis in vivo. Annu.Rev.Plant Biol. **59:** 89-113

Ballottari M, Truong TB, De Re E, Erickson E, Stella GR, Fleming GR, Bassi R, Niyogi KK (2016) Identification of pH-sensing Sites in the Light Harvesting Complex Stress-related 3 Protein Essential for Triggering Non-photochemical Quenching in Chlamydomonas reinhardtii. J Biol Chem **291:** 7334-7346

Bernaerts T, Gheysen L, Foubert I, Hendrickx M, Van Loey A (2019) The potential of microalgae and their biopolymers as structuring ingredients in food: A review. Biotechnology Advances **37**

Bonente G, Howes BD, Caffarri S, Smulevich G, Bassi R (2008) Interactions between the photosystem II subunit PsbS and xanthophylls studied in vivo and in vitro. J Biol Chem **283:** 8434-8445

Butler WL (1973) Primary photochemistry of photosystem II in photosynthesis. Acc.Chem.Res. **6:** 177-183

Camacho F, Macedo A, Malcata F (2019) Potential Industrial Applications and Commercialization of Microalgae in the Functional Food and Feed Industries: A Short Review. Marine Drugs **17**

Cao P, Pan X, Su X, Liu Z, Li M (2020) Assembly of eukaryotic photosystem II with diverse light-harvesting antennas. Curr Opin Struct Biol **63:** 49-57

Cazzaniga S, Kim M, Bellamoli F, Jeong J, Lee S, Perozeni F, Pompa A, Jin E, Ballottari M (2020) Photosystem II antenna complexes CP26 and CP29 are essential for nonphotochemical quenching in Chlamydomonas reinhardtii. Plant Cell and Environment **43:** 496-509

Croce R, Van Amerongen H (2011) Light-harvesting and structural organization of Photosystem II: from individual complexes to thylakoid membrane. J.Photochem.Photobiol.B **104:** 142-153

Dall'Osto L, Cazzaniga S, Zappone D, Bassi R (2020) Monomeric light harvesting complexes enhance excitation energy transfer from LHCII to PSII and control their lateral spacing in thylakoids. Biochim Biophys Acta Bioenerg **1861:** 148035

512 **de Bianchi S, Betterle N, Kouril R, Cazzaniga S, Boekema E, Bassi R, Dall'Osto L** (2011) Arabidopsis mutants
513 deleted in the light-harvesting protein Lhcb4 have a disrupted photosystem II macrostructure and
514 are defective in photoprotection. Plant Cell **23:** 2659-2679
515 **de Bianchi S, Dall'Osto L, Tognon G, Morosinotto T, Bassi R** (2008) Minor antenna proteins CP24 and
516 CP26 affect the interactions between photosystem II subunits and the electron transport rate
517 in grana membranes of Arabidopsis. Plant Cell **20:** 1012-1028
518 **Dinc E, Tian L, Roy LM, Roth R, Goodenough U, Croce R** (2016) LHCSR1 induces a fast and reversible pH-
519 dependent fluorescence quenching in LHCII in Chlamydomonas reinhardtii cells. Proc Natl Acad Sci
520 U S A **113:** 7673-7678
521 **Drop B, Webber-Birungi M, Yadav SK, Filipowicz-Szymanska A, Fusetti F, Boekema EJ, Croce R** (2014)
522 Light-harvesting complex II (LHCII) and its supramolecular organization in Chlamydomonas
523 reinhardtii. Biochim Biophys Acta **1837:** 63-72
524 **Elrad D, Niyogi KK, Grossman AR** (2002) A major light-harvesting polypeptide of photosystem II functions in
525 thermal dissipation. Plant Cell **14**
526 **Erickson E, Wakao S, Niyogi KK** (2015) Light stress and photoprotection in Chlamydomonas reinhardtii.
527 Plant J **82:** 449-465
528 **Garnier J, Maroc J, Guyon D** (1986) Low-temperature fluorescence emission spectra and chlorophyll-
529 protein complexes in mutants of Chlamydomonas reinhardtii: Evidence for a new chlorophyll-a-
530 protein complex related to photosystem I. Biochim.Biophys.Acta **851:** 395-406
531 **Genty B, Briantais J-M, Baker NR** (1989) The relationship between the quantum yield of photosynthetic
532 electron transport and quenching of chlorophyll fluorescence. Biochim.Biophys.Acta **990:** 87-92
533 **Girolomoni L, Ferrante P, Berteotti S, Giuliano G, Bassi R, Ballottari M** (2017) The function of LHCBM4/6/8
534 antenna proteins in Chlamydomonas reinhardtii. J Exp Bot **68:** 627-641
535 **Graham PJ, Nguyen B, Burdyny T, Sinton D** (2017) A penalty on photosynthetic growth in fluctuating light.
536 Sci Rep **7:** 12513
537 **Głowacka K, Kromdijk J, Kucera K, Xie J, Cavanagh AP, Leonelli L, Leakey ADB, Ort DR, Niyogi KK, Long SP**
538 (2018) Photosystem II Subunit S overexpression increases the efficiency of water use in a field-
539 grown crop. Nat Commun **9:** 868
540 **Hill R, Scarisbrick R** (1940) Production of Oxygen by Illuminated Chloroplasts. Nature **146:** 61
541 **Horton P** (1996) Nonphotochemical quenching of chlorophyll fluorescence. *In* RC Jennings, ed, Light as an
542 Energy Source and Information Carrier in Plant Physiology. New York, Plenum Press, pp 99-111
543 **Hyams J, Davies DR** (1972) The induction and characterisation of cell wall mutants of Chlamydomonas
544 reinhardi. Mutation Research/Fundamental and Molecular Mechanisms of Mutagenesis **14:** 381-
545 389
546 **Joo S, Kariyawasam T, Kim M, Jin E, Goodenough U, Lee JH** (2022) Sex-linked deubiquitinase establishes
547 uniparental transmission of chloroplast DNA. Nat Commun **13:** 1133
548 **Kim E, Akimoto S, Tokutsu R, Yokono M, Minagawa J** (2017) Fluorescence lifetime analyses reveal how the
549 high light-responsive protein LHCSR3 transforms PSII light-harvesting complexes into an energy-
550 dissipative state. J Biol Chem **292:** 18951-18960
551 **Kim E, Watanabe A, Duffy CDP, Ruban AV, Minagawa J** (2020) Multimeric and monomeric photosystem II
552 supercomplexes represent structural adaptations to low- and high-light conditions. J Biol Chem
553 **295:** 14537-14545
554 **Kim J, Lee S, Baek K, Jin E** (2020) Site-Specific Gene Knock-Out and On-Site Heterologous Gene
555 Overexpression in *Chlamydomonas reinhardtii* via a CRISPR-Cas9-Mediated Knock-in Method. Front
556 Plant Sci **11:** 306
557 **Koyande A, Chew K, Rambabu K, Tao Y, Chu D, Show P** (2019) Microalgae: A potential alternative to health
558 supplementation for humans. Food Science and Human Wellness **8:** 16-24
559 **Kromdijk J, Glowacka K, Leonelli L, Gabilly ST, Iwai M, Niyogi KK, Long SP** (2016) Improving photosynthesis
560 and crop productivity by accelerating recovery from photoprotection. Science **354:** 857-861
561 **Kropat J, Hong-Hermesdorf A, Casero D, Ent P, Castruita M, Pellegrini M, Merchant S, Malasarn D** (2011)
562 A revised mineral nutrient supplement increases biomass and growth rate in Chlamydomonas
563 reinhardtii. Plant Journal **66:** 770-780

564 **Lagarde D, Beuf L, Vermaas W** (2000) Increased production of zeaxanthin and other pigments by
565 application of genetic engineering techniques to Synechocystis sp. strain PCC 6803. Appl Environ
566 Microbiol **66:** 64-72
567 **Liguori N, Novoderezhkin V, Roy LM, van Grondelle R, Croce R** (2016) Excitation dynamics and structural
568 implication of the stress-related complex LHCSR3 from the green alga Chlamydomonas reinhardtii.
569 Biochim Biophys Acta **1857:** 1514-1523
570 **Liguori N, Roy LM, Opacic M, Durand G, Croce R** (2013) Regulation of light harvesting in the green alga
571 Chlamydomonas reinhardtii: the C-terminus of LHCSR is the knob of a dimmer switch. J Am Chem
572 Soc **135:** 18339-18342
573 **Long SP, Humphries S, Falkowski PG** (1994) Photoinhibition of photosynthesis in nature. Ann.Rev.Plant
574 Physiol.Plant Mol.Biol. **45:** 633-662
575 **Malkin S, Armond PA, Mooney HA, Fork DC** (1981) Photosystem II Photosynthetic Unit Sizes from
576 Fluorescence Induction in Leaves : CORRELATION TO PHOTOSYNTHETIC CAPACITY. Plant Physiol **67:**
577 570-579
578 **Medipally SR, Yusoff FM, Banerjee S, Shariff M** (2015) Microalgae as Sustainable Renewable Energy
579 Feedstock for Biofuel Production. Biomed Res Int **2015:** 519513
580 **Minagawa J, Takahashi Y** (2004) Structure, function and assembly of Photosystem II and its light-harvesting
581 proteins. Photosynth Res **82:** 241-263
582 **Natali A, Croce R** (2015) Characterization of the major light-harvesting complexes (LHCBM) of the green
583 alga Chlamydomonas reinhardtii. PLoS One **10:** e0119211
584 **Neidhardt J, Benemann JR, Zhang LP, Melis A** (1998) Photosystem-II repair and chloroplast recovery from
585 irradiance stress: relationship between chronic photoinhibition, light-harvesting chlorophyll
586 antenna size and photosynthetic productivity in Dunaliella salina (green algae). Photosynthesis
587 Research **56:** 175-184
588 **Nelson N, Ben Shem A** (2004) The complex architecture of oxygenic photosynthesis. Nature **5:** 1-12
589 **Niyogi KK, Truong TB** (2013) Evolution of flexible non-photochemical quenching mechanisms that regulate
590 light harvesting in oxygenic photosynthesis. Curr Opin Plant Biol **16:** 307-314
591 **Peers G, Truong TB, Ostendorf E, Busch A, Elrad D, Grossman AR, Hippler M, Niyogi KK** (2009) An ancient
592 light-harvesting protein is critical for the regulation of algal photosynthesis. Nature **462:** 518-521
593 **Perozeni F, Cazzaniga S, Baier T** (2020) Turning a green alga red: engineering astaxanthin biosynthesis by
594 intragenic pseudogene revival in Chlamydomonas reinhardtii. **18:** 2053-2067
595 **Perozeni F, Cazzaniga S, Baier T, Zanoni F, Zoccatelli G, Lauersen K, Wobbe L, Ballottari M** (2020) Turning a
596 green alga red: engineering astaxanthin biosynthesis by intragenic pseudogene revival in
597 Chlamydomonas reinhardtii. Plant Biotechnology Journal **18:** 2053-2067
598 **Peter GF, Takeuchi T, Thornber JP** (1991) Solubilization and two-dimensional electrophoretic procedures
599 for studying the organization and composition of photosynthetic membrane polypeptides.
600 Methods: A Companion to Methods in Enzymology **3:** 115-124
601 **Rani A, Saini KC, Bast F, Mehariya S, Bhatia SK, Lavecchia R, Zuorro A** (2021) Microorganisms: A Potential
602 Source of Bioactive Molecules for Antioxidant Applications. Molecules **26**
603 **Sacharz J, Giovagnetti V, Ungerer P, Mastroianni G, Ruban AV** (2017) The xanthophyll cycle affects
604 reversible interactions between PsbS and light-harvesting complex II to control non-photochemical
605 quenching. Nat Plants **3:** 16225
606 **Schägger H, von Jagow G** (1987) Tricine-sodium dodecyl sulfate-polyacrylamide gel electrophoresis for the
607 separation of proteins in the range from 1 to 100 kDa. Anal.Biochem. **166:** 368-379
608 **Semchonok DA, Sathish Yadav KN, Xu P, Drop B, Croce R, Boekema EJ** (2017) Interaction between the
609 photoprotective protein LHCSR3 and C2S2 Photosystem II supercomplex in Chlamydomonas
610 reinhardtii. Biochim Biophys Acta **1858:** 379-385
611 **Shen L, Huang Z, Chang S, Wang W, Wang J, Kuang T, Han G, Shen J-R, Zhang X** (2019) Structure of a
612 C2S2M2N2-type PSII–LHCII supercomplex from the green alga Chlamydomonas reinhardtii.
613 Proceedings of the National Academy of Sciences **116:** 21246-21255
614 **Suga M, Akita F, Hirata K, Ueno G, Murakami H, Nakajima Y, Shimizu T, Yamashita K, Yamamoto M, Ago**
615 **H, Shen JR** (2015) Native structure of photosystem II at 1.95 A resolution viewed by femtosecond X-
616 ray pulses. Nature **517:** 99-103

Tian L, Nawrocki Wojciech J, Liu X, Polukhina I, van Stokkum Ivo HM, Croce R (2019) pH dependence, kinetics and light-harvesting regulation of nonphotochemical quenching in Chlamydomonas. Proceedings of the National Academy of Sciences **116:** 8320-8325

Tokutsu R, Kato N, Bui KH, Ishikawa T, Minagawa J (2012) Revisiting the supramolecular organization of photosystem II in Chlamydomonas reinhardtii. J Biol Chem **287:** 31574-31581

Tokutsu R, Minagawa J (2013) Energy-dissipative supercomplex of photosystem II associated with LHCSR3 in Chlamydomonas reinhardtii. Proc Natl Acad Sci U S A **110:** 10016-10021

Troiano JM, Perozeni F, Moya R, Zuliani L, Baek K, Jin E, Cazzaniga S, Ballottari M, Schlau-Cohen GS (2021) Identification of distinct pH- and zeaxanthin-dependent quenching in LHCSR3 from Chlamydomonas reinhardtii. Elife **10**

Van Kooten O, Snel JFH (1990) The use of chlorophyll fluorescence nomenclature in plant stress physiology. Photosynt.Res. **25:** 147-150

Vass I, Styring S, Hundal T, Koivuniemi A, Aro E-M, Andersson B (1992) Reversible and irreversible intermediates during photoinhibition of photosystem II: Stable reduced QA species promote chlorophyll triplet formation. Proc.Natl.Acad.Sci.USA **89:** 1408-1412

ACKNOWLEDGEMENTS

The research was supported by the ERC (European Research Council) Starting Grant SOLENALGAE (679814) to M.B. and by Basic Science Research Program (NRF2020R1A2C2011998) and Carbon to X Project (2020M3H7A1098294) of the National Research Foundation (NRF) of Korea, funded by the Korean government. to E.J.

AUTHOR CONTRIBUTIONS

MB designed the research. EJ coordinated the research activity for generation of mutant strains and contributed to experiment design. CD coordinated the research activity for time resolved fluorescence analysis of whole cells. SC, MK, SS, FP and MP performed experiments. All the authors analyzed data. SC, EJ and MB wrote the paper. All the authors discussed the results, contributed to data interpretation, commented on the manuscript and approved its final version.

Authors declare no conflict of interest

651 **SUPPLEMENTAL MATERIAL**

652 **Figure S1. Screening and verification of CP26 knock out mutants.**

653 **Figure S2. CP26 immunotitration in *k9* mutant.**

654 **Figure S3. F_0 and F_m fluorescence normalized to chlorophyll content.**

655 **Figure S4. Photosynthetic parameters in *k9* and *k69-***

656 **Figure S5. Growth curves for *k9* and *k69*.**

657 **Figure S6. Immunotitration of LHCSR proteins per PSII.**

658 **Figure S7 Nonphotochemical quenching at different actinic lights.**

659 **Figure S8. Nonphotochemical quenching in *k9* and *k69* mutants**

660 **Figure S9. Acid induced quenching in 4a+ and *npq4 lhcsr1***

661 **Figure S10. Acid induced quenching in *k9* and *k69*.**

662 **Figure S11. *k6* mutant complementation.**

663 **Figure S12. *k6* line complemented with CP26**.

664 **Table S1. Sanger sequencing of the CP26 knock-out mutants.**

665 **Table S2. Fluorescence lifetimes of whole *Chlamydomonas reinhardtii* cells.**

666 **Table S3 Light curve parameters and respiration rates.**

667

668

669

670

671 **TABLES**

672 **Table 1 Pigment analysis and Fv/Fm.** Data were collected from cells grown in photoautotrophy at 80-100
673 µmol photons m-2 s-1. Single carotenoids values were normalized to 100 chlorophylls. Data are expressed as
674 mean ± SD. (n = 4). Values that are significantly different (Student's t-test, P < 0.05) from the wild-type
675 (Wt) are marked with an asterisk (*). Abbreviations: Chl, chlorophyll; Car, carotenoids; Neo, neoxanthin;
676 Lor, loroxanthin; viola, violaxanthin; Ant, anteraxanthin; Lut, lutein; β-Car, β-Carotene.

677

678

					Car/100 Chl					
	Chl (pg)/cell	**Chl a/b**	**Chl/Car**	**Fv/Fm**	**Neo**	**Lor**	**Viol**	**Ant**	**lut**	β-Car
Wt	1.40 ± 0.07	2.65 ± 0.04	3.16 ± 0.07	0.72 ± 0.01	3.43 ± 0.59	5.12 ± 0.36	3.30 ± 0.08	0.39 ± 0.04	13.85 ± 0.50	4.42 ± 0.71
k6	1.47 ± 0.22	2.48 ± 0.04	3.16 ± 0.03	0.67 ± 0.02*	3.60 ± 0.96	3.99 ± 0.37	3.23 ± 0.27	0.15 ± 0.14	15.03 ± 0.90	4.21 ± 0.47

679

680

681

682 **FIGURE LEGENDS**

683

684 **Figure 1. CP26 knock-out by CRISPR/Cas9 genome editing.** (a) Location of the Cas9 target site in the
685 CP26 gene. Light gray colored- and dark gray colored-box indicate UTR regions and exons, respectively.
686 The nucleotides highlighted in yellow and red indicate the sgRNA sequence and its' PAM sequence,
687 respectively. Black arrows indicate the primer sets for colony PCR (b) Colony PCR of the selected CP26
688 knock-out mutants using the specific primers designed near the Cas9 target site of CP26. (c) Sanger
689 sequencing of the selected CP26 knock-out mutants. In/del values represent inserted or deleted nucleotides in
690 sgRNA target site of CP26 in wild-type (WT). Hygromycin-resistance gene (HygR/ aphVII) cassette inserted
691 in the target cited of CP26 gene was identified with either forward (F) or reverse (R) orientation. The size of
692 the HygR cassette is 1,624 bp. The deleted sequence in the sgRNA target site was highlighted by a gray-
693 colored line (d) Immunoblot analysis of the four selected CP26 knock-out mutants with a specific antibody
694 directed against CP26. Immunoblot against CP43 was added as loading control (e) SDS-PAGE analysis of
695 thylakoid isolated from WT and *k6* performed with the Tris-Tricine buffer system. Fifteen micrograms of
696 Chl were loaded in each lane. Molecular weight (MW) markers are indicated on the left. Blue arrows
697 indicate the position of monomeric antenna CP29 (upper arrow) and CP26 (lower arrow) on the SDS-PAGE.

698 **Figure 2. Organization of the photosynthetic complexes.** (a) Immunotitration of wild-type (Wt) and *k6*
699 thylakoid proteins using specific antibodies against PSI core (PSAA), LHCII and CP29. Data were corrected
700 for CP43 amount and normalized to Wt ratio. LHCII is shown as total amount (LHCII) or divided for three
701 bands that are separated on the Tris-Tricine buffer system. Data are expressed as mean ± SD. (n = 4). *k6*
702 values that are significantly different (Student's t-test, $P < 0.05$) from the Wt are marked with an asterisk (*).
703 (b) Image of western blot used for the Immunotitration. Specific antibodies were used on cellulose lanes
704 loaded with 2, 1, 0.5 and 0.25 µg of Chls. (c) Thylakoid pigment-binding complexes were separated by non-
705 denaturing Deriphat-PAGE upon solubilization with 0.8% α-dodecyl-maltoside. Thylakoids corresponding to
706 30 µg of Chls were loaded in each lane. Composition of each band is indicated.

707 **Figure 3. Light harvesting**. (a) Low-temperature fluorescence emission spectra of wild-type (Wt, black)
708 and *k6* (red) cells excited at 475 nm. Emission spectra are normalized at the maximum emission on PSII
709 peak. Data are expressed as mean ± SD (n = 4) indicated on the PSI peak. (b) Variable Chl fluorescence was
710 induced with a weak red light on dark-adapted cells ($2 \cdot 10^6$ cells/ml) in presence of 50 µM of DCMU. The
711 trace for Wt and *k6* are the average of 12 curve from three different experiments. The reciprocal of time
712 corresponding to two-thirds of the fluorescence rise ($1/\tau_{2/3}$) is as a measure of the PSII functional antenna
713 size and it is shown in the inset normalized to the Wt. (c) Time-resolved fluorescence decays of Wt and *k6*
714 whole cells

715 **Figure 4. Photosynthetic electron flow.** Dependence of the (a) PSII operating efficiency (ΦPSII), (b)
716 relative electron transport rate (ETR), (c) 1-qL (reduced Q_A fraction), and (d) photosynthetic O2 evolution on
717 actinic light intensity for wild type (Wt, black) and *k6* (red). Net photosynthetic rate data were fitted with
718 Hill equation. Data are expressed as mean ± SD. $n > 3$. *k6* values that are significantly different (Student's t-
719 test, $P < 0.05$) from Wt are marked with an asterisk (*).

720 **Figure 5. Growth curves under autotrophic conditions.** Wild-type (Wt, black) and *k6* (red) where grown
721 at (a) low (30-40 µmol m^{-2} s^{-1},LL), (b) control (100-120 µmol m^{-2} s^{-1},CL) or (c) high light (700-800 µmol
722 m^{-2} s^{-1},HL) and the cell content was measured. Growth curves were fitted with Hill equation. (d) specific
723 growth rate (µ) calculated for all the different light conditions. Error bars are reported as standard deviation
724 ($n > 3$). *k6* values that are significantly different (Student's t-test, $P < 0.05$) from Wt are marked with an
725 asterisk (*).

Figure 6. Nonphotochemical quenching. (a) Measurement of NPQ kinetic on wild-type (Wt, black) and *k6* (red) cells using actinic lights of 1,200 µmol photons m^{-2} s^{-1}. (b) NPQ value after 15 min of illumination at different actinic light intensities. Error bars are reported as standard deviation (n >4).

Figure 7. Acid induced quenching. (a,b) PAM Chl fluorometer trace of wild-type (Wt) (a) and *k6* (b) before and after acidification with acetic acid. The back arrow indicates when the acid was added. Fluorescence was recorded in the dark with two saturating pulses before and two after the acidification. (c) NPQ calculated for each trace as $(Fm-Fm^A)/Fm^A$ where Fm and Fm^A are the fluorescence before and after acidification. Error bars are reported as standard deviation (n > 3). *k6* values that are significantly different (Student's t-test, $P < 0.05$) from Wt are marked with an asterisk (*).

Figure 8. Nonphotochemical quenching in *k6* complemented line. (a) NPQ using an actinic light of 1,200 µmol m^{-2} s^{-1} in five *k6* lines complemented with CP26. The selected lines (named *k6c#*) accumulate CP26 to the same level as the wild-type. Wil-type (Wt, black) and *k6* (red) NPQ was added as reference. (b) Correlation between the amount of CP26 and the NPQ reached after 15 minutes of illumination with actinic light at 1200 µmol m^{-2} s^{-1}. *k6c#* are indicate as blue triangles, Wt as a black square and *k6* as a red circle.

763

764

765

766

767

768 **FIGURES**

769 **Figure 1**

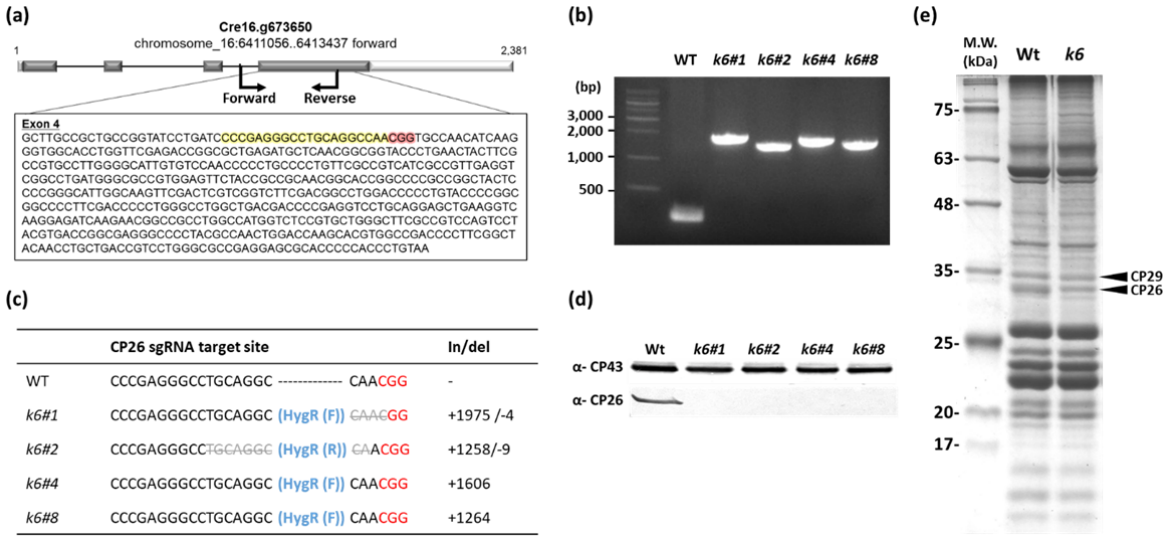

	CP26 sgRNA target site	In/del
WT	CCCGAGGGCCTGCAGGC ---------- CAACGG	-
k6#1	CCCGAGGGCCTGCAGGC (HygR (F)) ~~GAAG~~GG	+1975 /-4
k6#2	CCCGAGGGCC~~TGCAGGC~~ (HygR (R)) ~~CA~~ACGG	+1258/-9
k6#4	CCCGAGGGCCTGCAGGC (HygR (F)) CAACGG	+1606
k6#8	CCCGAGGGCCTGCAGGC (HygR (F)) CAACGG	+1264

770

771

772

773

774

775

776

777

778

779

780

781

782

783

784

785

786

Figure 2

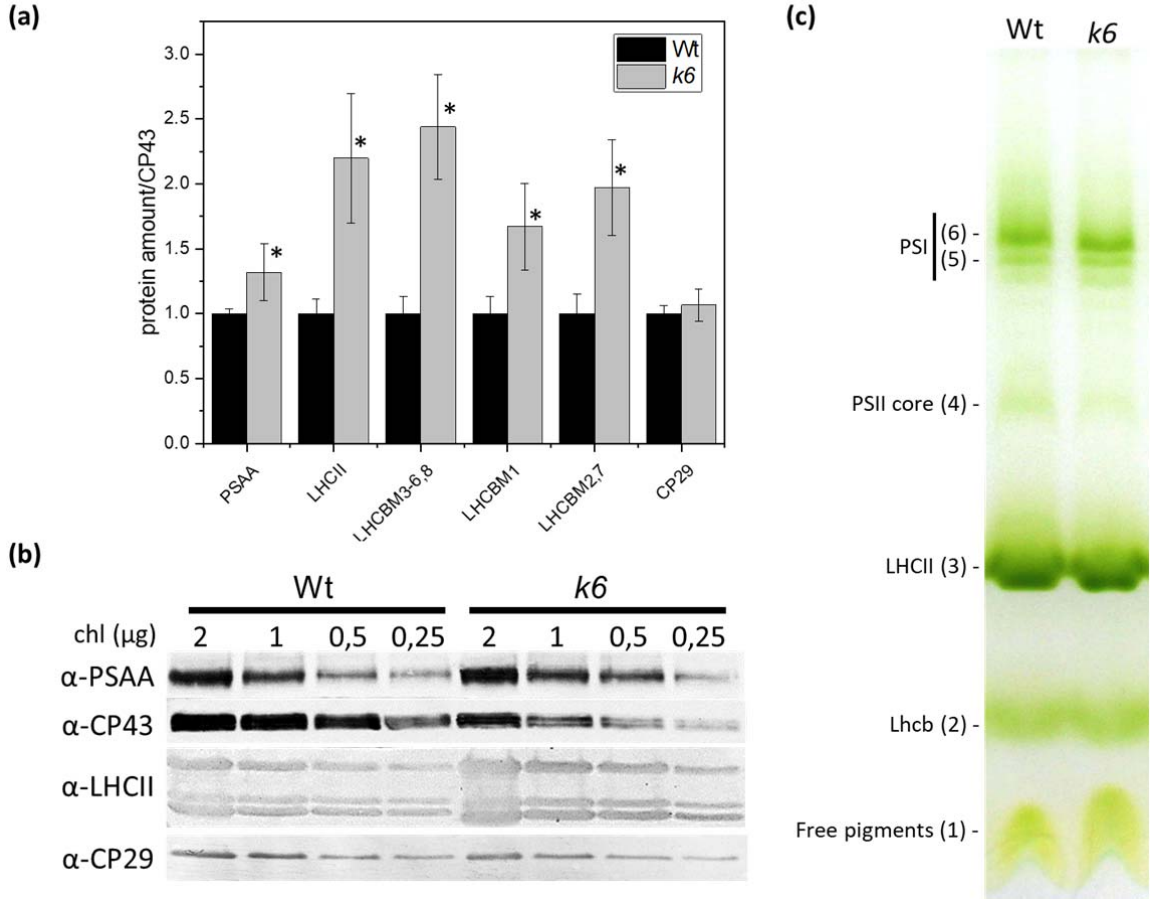
(a)
protein amount/CP43
Wt
k6
PSAA
LHCII
LHCBM3-6,8
LHCBM1
LHCBM2,7
CP29
(b)
Wt
k6
chl (µg)
2
1
0,5
0,25
α-PSAA
α-CP43
α-LHCII
α-CP29
(c)
Wt
k6
PSI
(6) -
(5) -
PSII core (4) -
LHCII (3) -
Lhcb (2) -
Free pigments (1) -

Figure 3

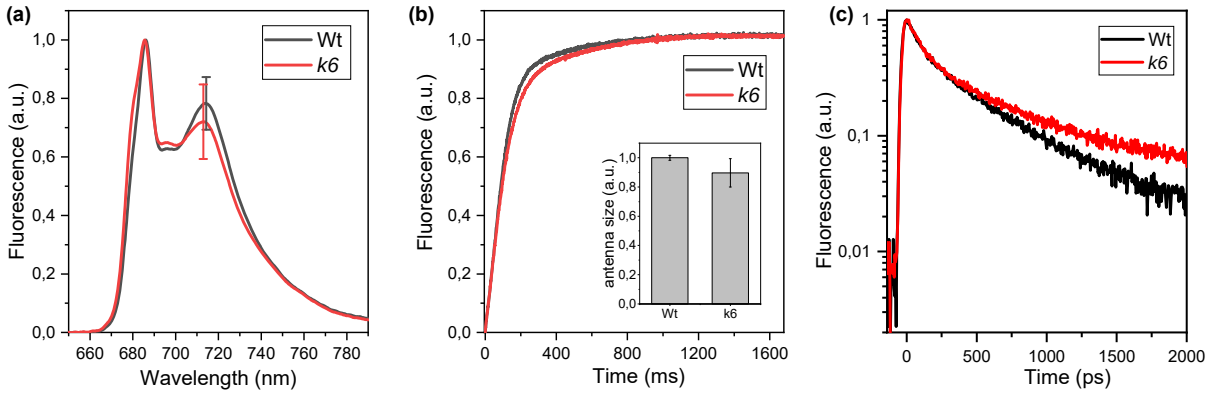
(a)
Wt
k6
Fluorescence (a.u.)
Wavelength (nm)
(b)
Wt
k6
Fluorescence (a.u.)
Time (ms)
antenna size (a.u.)
Wt
k6
(c)
Wt
k6
Fluorescence (a.u.)
Time (ps)

Figure 4

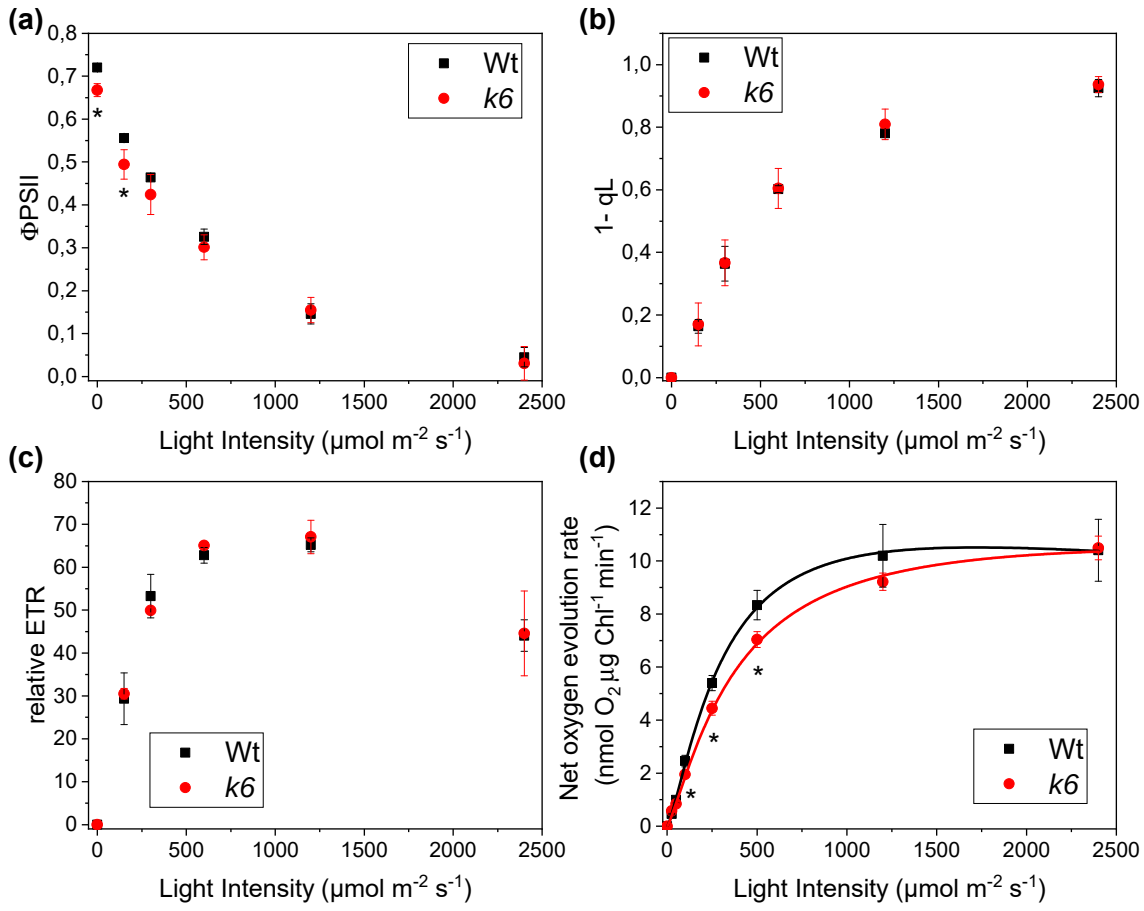
(a)
ΦPSII
Wt
k6
Light Intensity (µmol m-2 s-1)
(b)
1- qL
Wt
k6
Light Intensity (µmol m-2 s-1)
(c)
relative ETR
Wt
k6
Light Intensity (µmol m-2 s-1)
(d)
Net oxygen evolution rate
(nmol O2 µg Chl-1 min-1)
Wt
k6
Light Intensity (µmol m-2 s-1)

Figure 5

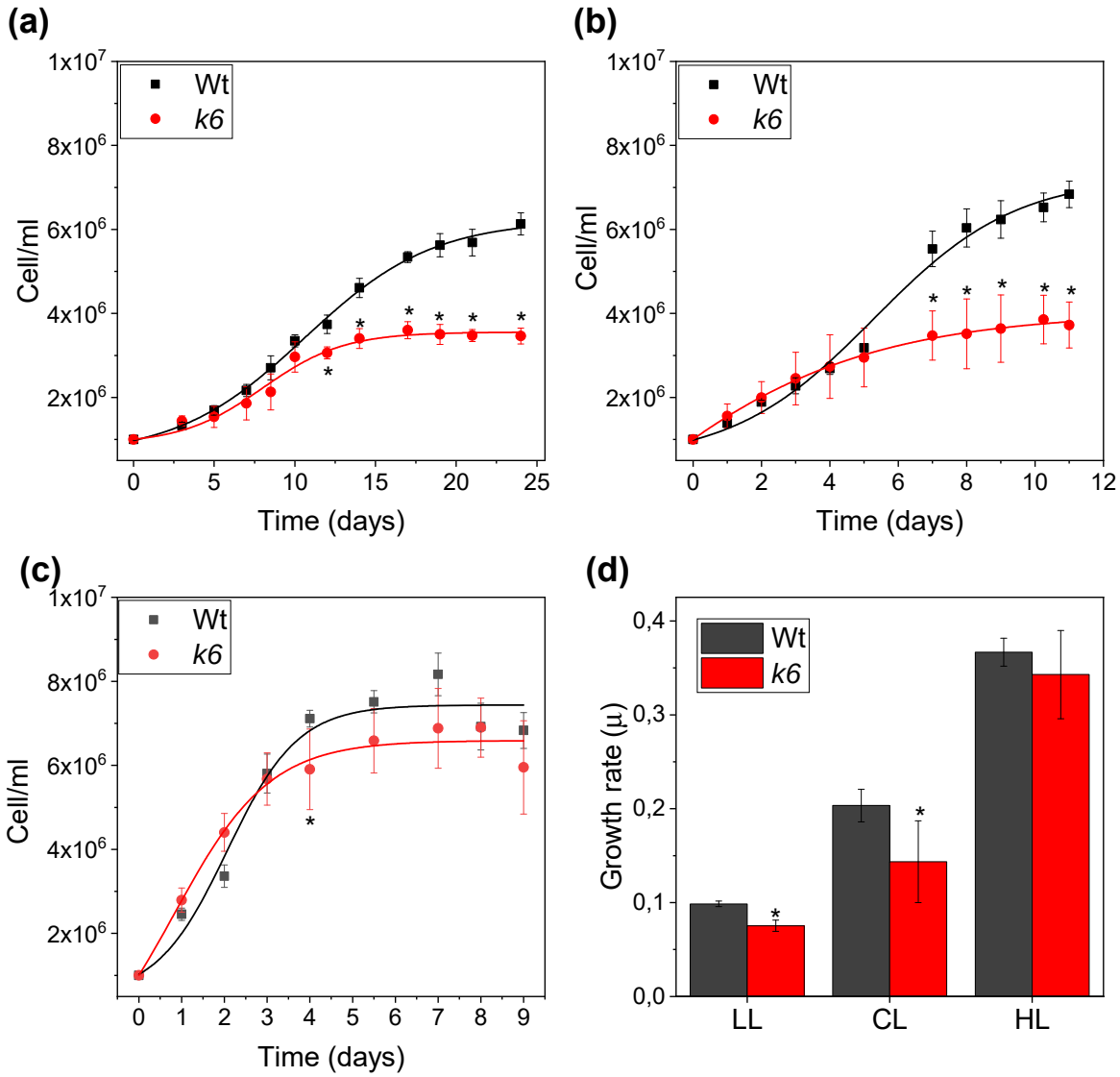

Figure 6

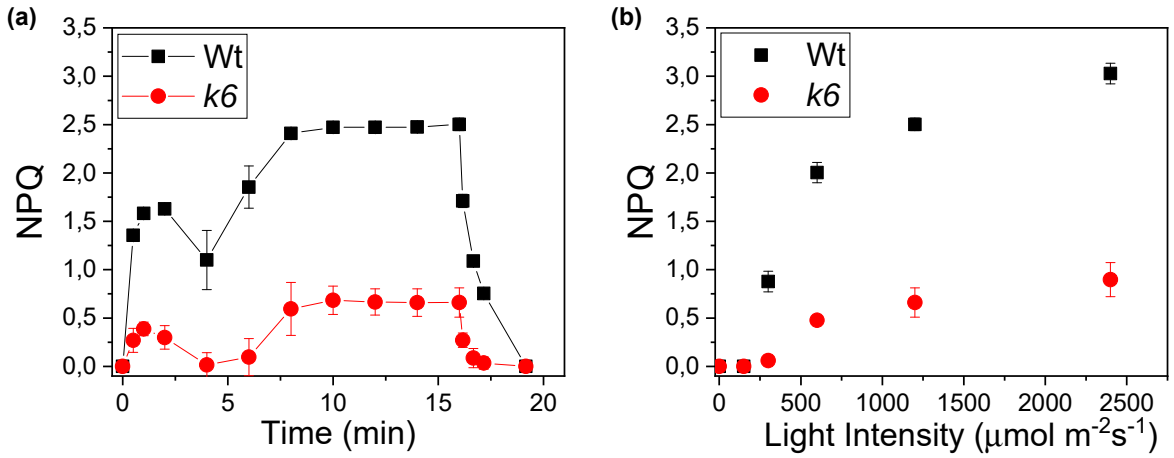

883
884
885
886
887
888
889
890 Figure 7
891

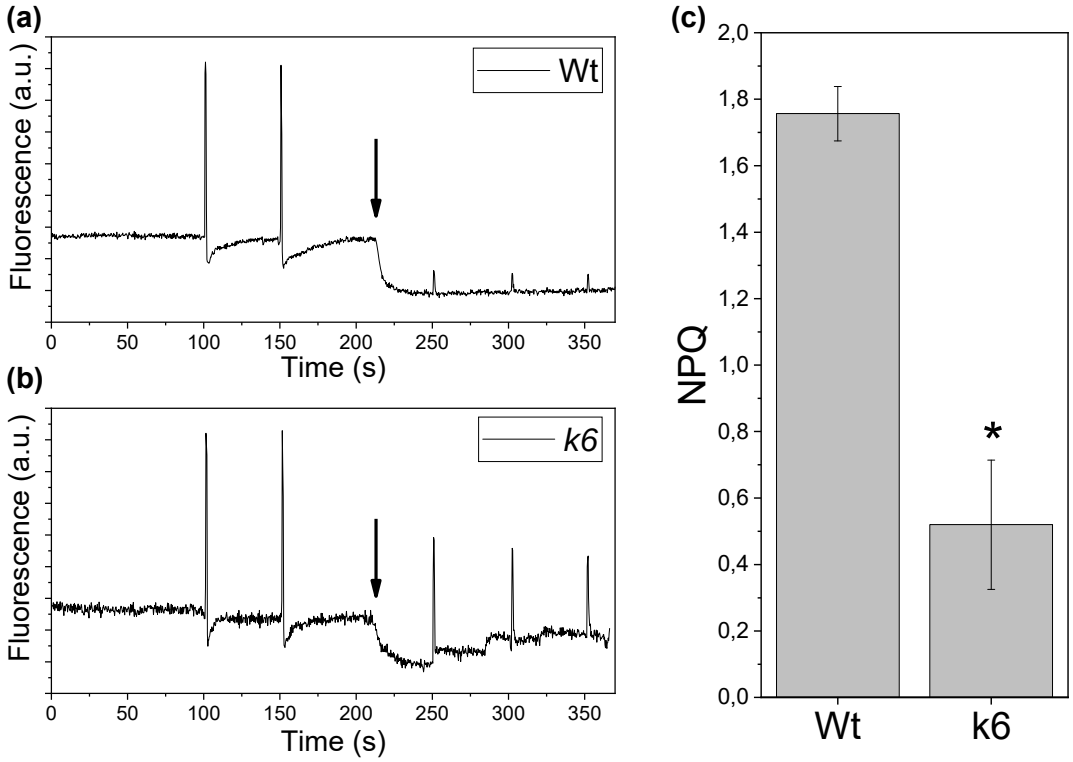

892
893
894
895
896
897
898
899
900
901

Figure 8

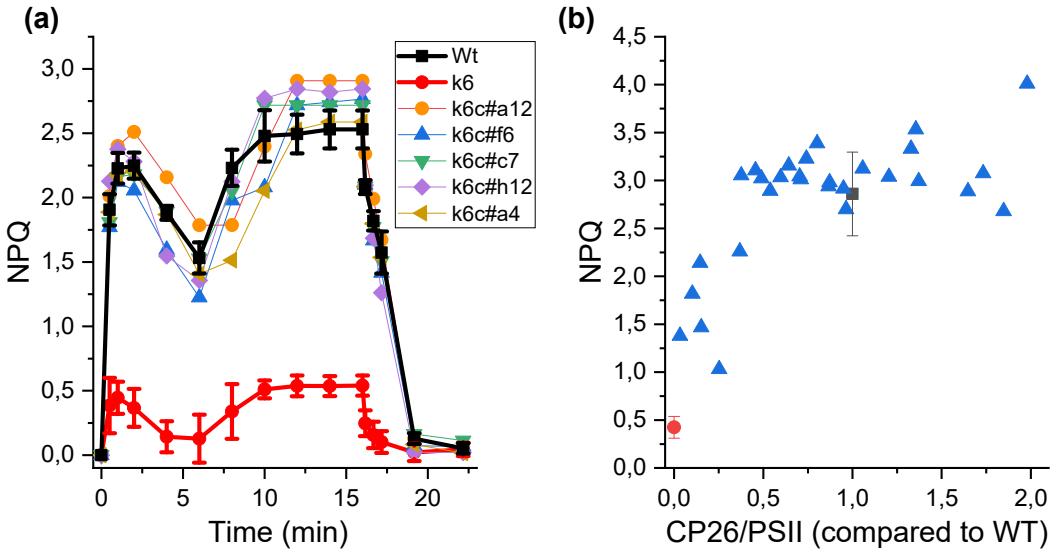
(a)
NPQ
Time (min)
Wt
k6
k6c#a12
k6c#f6
k6c#c7
k6c#h12
k6c#a4
(b)
NPQ
CP26/PSII (compared to WT)

Figure 1

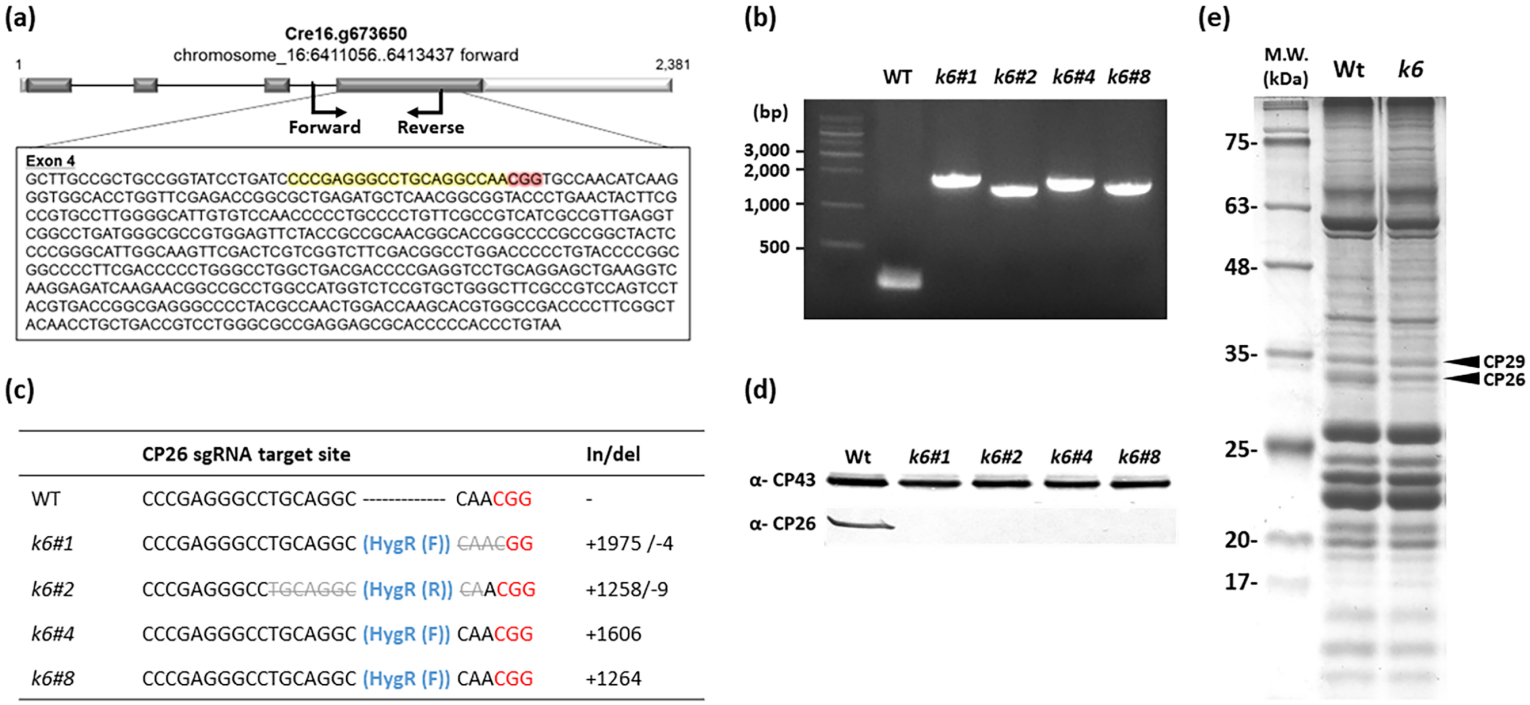

	CP26 sgRNA target site	In/del
WT	CCCGAGGGCCTGCAGGC ---------- CAACGG	-
k6#1	CCCGAGGGCCTGCAGGC (HygR (F)) ~~CAAC~~GG	+1975 /-4
k6#2	CCCGAGGGCC~~TGCAGGC~~ (HygR (R)) ~~CA~~ACGG	+1258/-9
k6#4	CCCGAGGGCCTGCAGGC (HygR (F)) CAACGG	+1606
k6#8	CCCGAGGGCCTGCAGGC (HygR (F)) CAACGG	+1264

Figure 1. CP26 knock-out by CRISPR/Cas9 genome editing. (a) Location of the Cas9 target site in the CP26 gene. Light gray colored- and dark gray colored-box indicate UTR regions and exons, respectively. The nucleotides highlighted in yellow and red indicate the sgRNA sequence and its' PAM sequence, respectively. Black arrows indicate the primer sets for colony PCR (b) Colony PCR of the selected CP26 knock-out mutants using the specific primers designed near the Cas9 target site of CP26. (c) Sanger sequencing of the selected CP26 knock-out mutants. In/del values represent inserted or deleted nucleotides in sgRNA target site of CP26 in wild-type (WT). Hygromycin-resistance gene (HygR/ aphVII) cassette inserted in the target cited of CP26 gene was identified with either forward (F) or reverse (R) orientation. The size of the HygR cassette is 1,624 bp. The deleted sequence in the sgRNA target site was highlighted by a gray-colored line (d) Immunoblot analysis of the four selected CP26 knock-out mutants with a specific antibody directed against CP26. Immunoblot against CP43 was added as loading control (e) SDS-PAGE analysis of thylakoid isolated from WT and *k6* performed with the Tris-Tricine buffer system. Fifteen micrograms of Chl were loaded in each lane. Molecular weight (MW) markers are indicated on the left. Blue arrows indicate the position of monomeric antenna CP29 (upper arrow) and CP26 (lower arrow) on the SDS-PAGE.

Figure 2

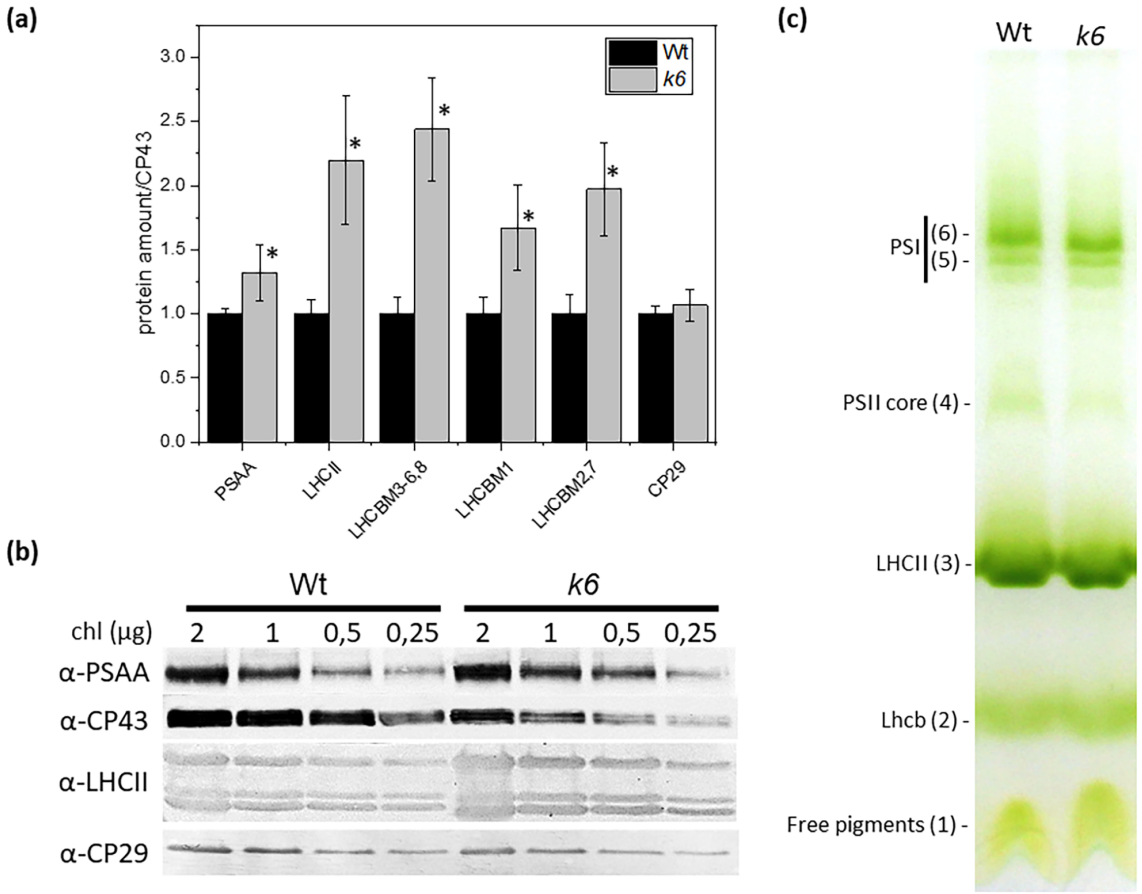

Figure 2. Organization of the photosynthetic complexes. (a) Immunotitration of wild-type (Wt) and *k6* thylakoid proteins using specific antibodies against PSI core (PSAA), LHCII and CP29. Data were corrected for CP43 amount and normalized to Wt ratio. LHCII is shown as total amount (LHCII) or divided for three bands that are separated on the Tris-Tricine buffer system. Data are expressed as mean ± SD. (n = 4). *k6* values that are significantly different (Student's t-test, $P < 0.05$) from the Wt are marked with an asterisk (*). (b) Image of western blot used for the Immunotitration. Specific antibodies were used on cellulose lanes loaded with 2, 1, 0.5 and 0.25 µg of Chls. (c) Thylakoid pigment-binding complexes were separated by non-denaturing Deriphat-PAGE upon solubilization with 0.8% α-dodecyl-maltoside. Thylakoids corresponding to 30 µg of Chls were loaded in each lane. Composition of each band is indicated.

Figure 3

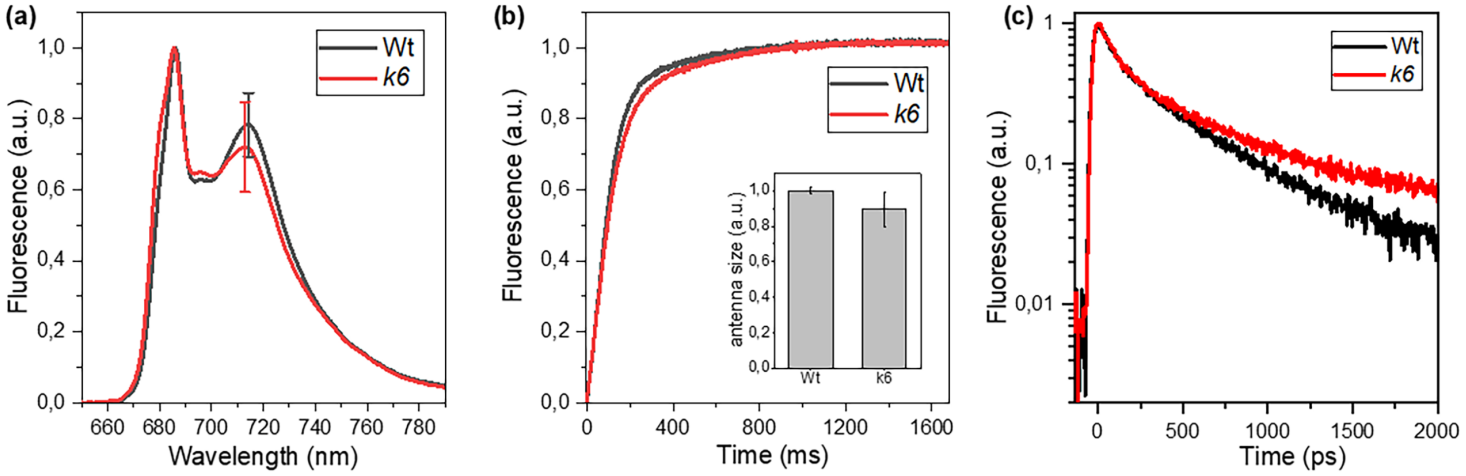

Figure 3. Light harvesting. (a) Low-temperature fluorescence emission spectra of wild-type (Wt, black) and *k6* (red) cells excited at 475 nm. Emission spectra are normalized at the maximum emission on PSII peak. Data are expressed as mean ± SD (n = 4) indicated on the PSI peak. (b) Variable Chl fluorescence was induced with a weak red light on dark-adapted cells ($2 \cdot 10^6$ cells/ml) in presence of 50 µM of DCMU. The trace for Wt and *k6* are the average of 12 curve from three different experiments. The reciprocal of time corresponding to two-thirds of the fluorescence rise ($1/\tau_{2/3}$) is as a measure of the PSII functional antenna size and it is shown in the inset normalized to the Wt. (c) Time-resolved fluorescence decays of Wt and *k6* whole cells

Figure 4

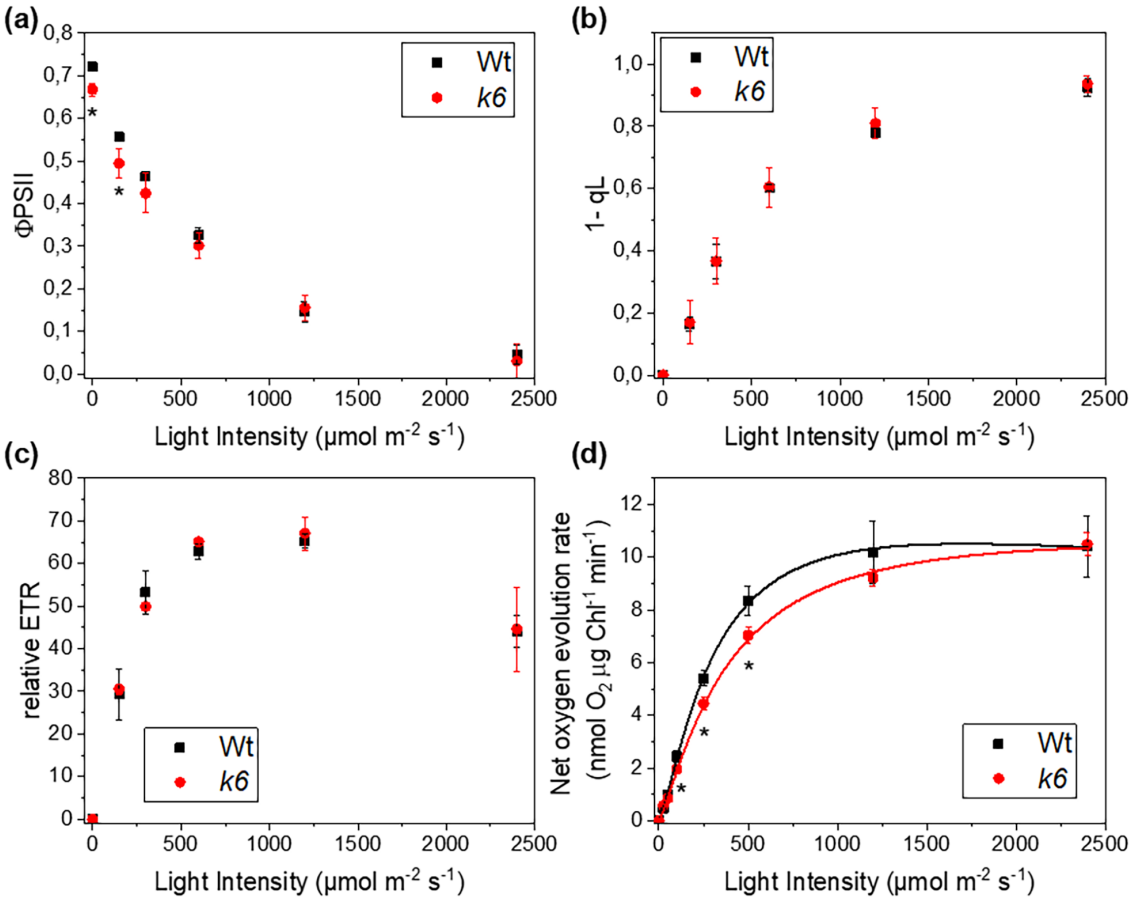

Figure 4. Photosynthetic electron flow. Dependence of the (a) PSII operating efficiency (ΦPSII), (b) relative electron transport rate (ETR), (c) 1-qL (reduced Q_A fraction), and (d) photosynthetic O2 evolution on actinic light intensity for wild type (Wt, black) and k6 (red). Net photosynthetic rate data were fitted with Hill equation. Data are expressed as mean ± SD. n > 3. *k6* values that are significantly different (Student's t-test, $P < 0.05$) from Wt are marked with an asterisk (*).

Figure 5

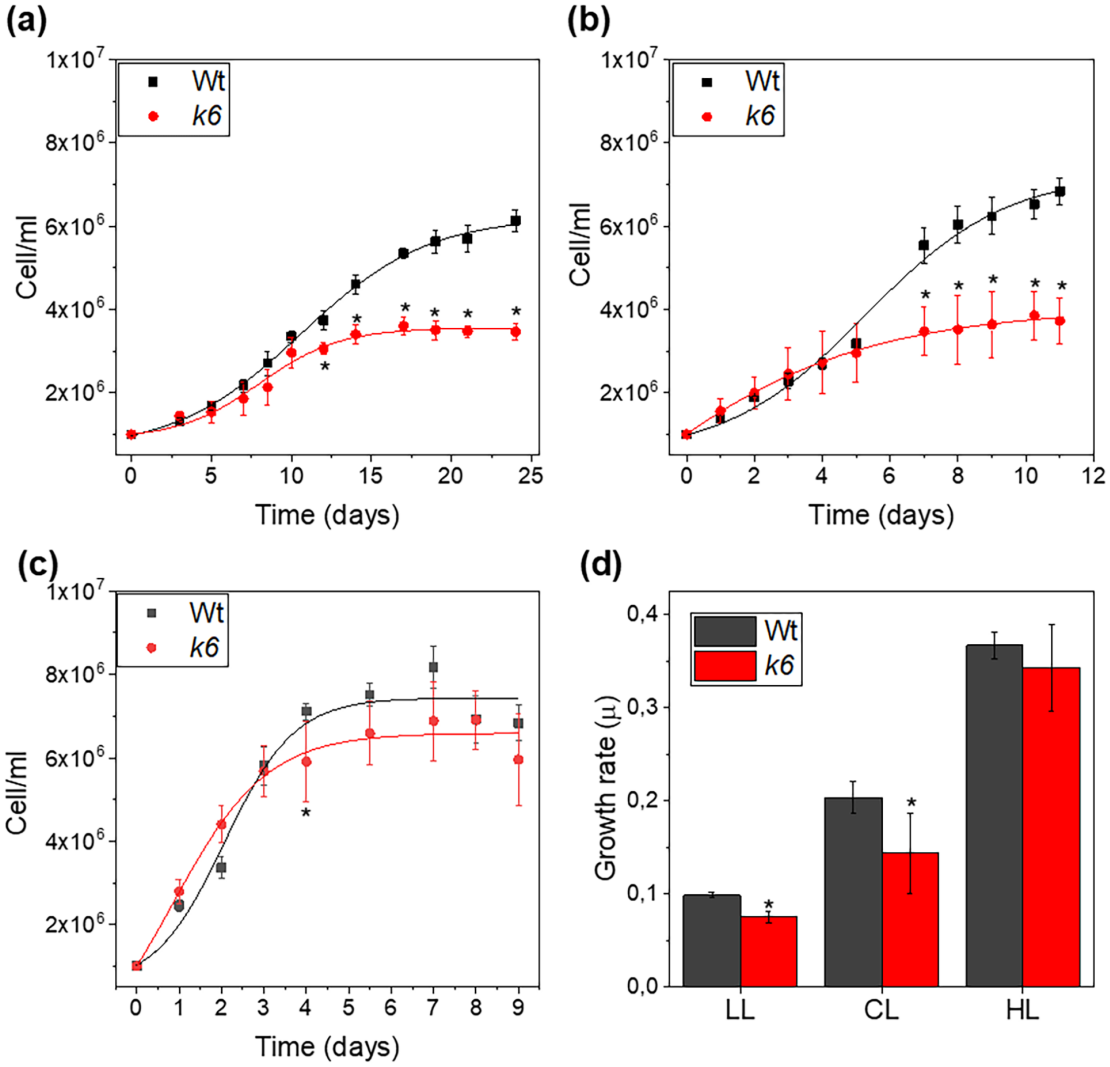

Figure 5. Growth curves under autotrophic conditions. Wild-type (Wt, black) and *k6* (red) where grown at (a) low (30-40 μmol m^{-2} s^{-1},LL), (b) control (100-120 μmol m^{-2} s^{-1},CL) or (c) high light (700-800 μmol m^{-2} s^{-1},HL) and the cell content was measured. Growth curves were fitted with Hill equation. (d) specific growth rate (μ) calculated for all the different light conditions. Error bars are reported as standard deviation ($n > 3$). *k6* values that are significantly different (Student's t-test, $P < 0.05$) from Wt are marked with an asterisk (*).

Figure 6

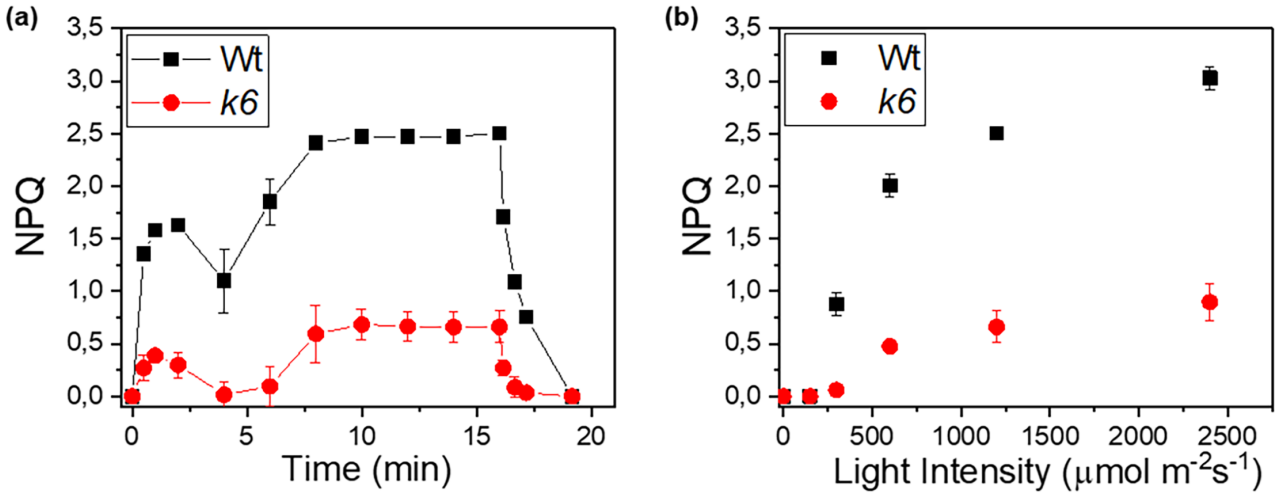

Figure 6. Nonphotochemical quenching. (a) Measurement of NPQ kinetic on wild-type (Wt, black) and *k6* (red) cells using actinic lights of 1,200 µmol photons m^{-2} s^{-1}. (b) NPQ value after 15 min of illumination at different actinic light intensities. Error bars are reported as standard deviation (n >4).

Figure 7

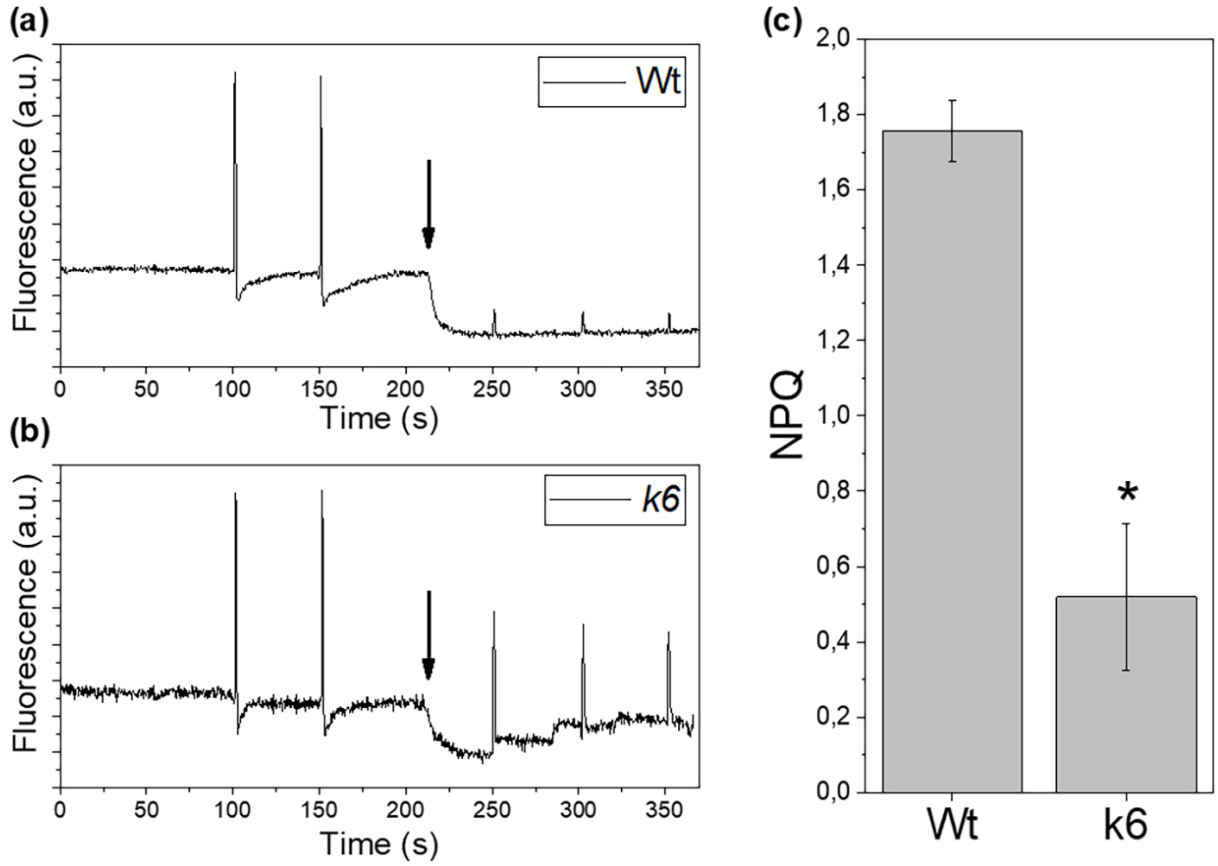

Figure 7. Acid induced quenching. (a,b) PAM Chl fluorometer trace of wild-type (Wt) (a) and *k6* (b) before and after acidification with acetic acid. The back arrow indicates when the acid was added. Fluorescence was recorded in the dark with two saturating pulses before and two after the acidification. (c) NPQ calculated for each trace as $(Fm-Fm^A)/Fm^A$ where Fm and Fm^A are the fluorescence before and after acidification. Error bars are reported as standard deviation ($n > 3$). *k6* values that are significantly different (Student's t-test, $P < 0.05$) from Wt are marked with an asterisk (*).

Figure 8

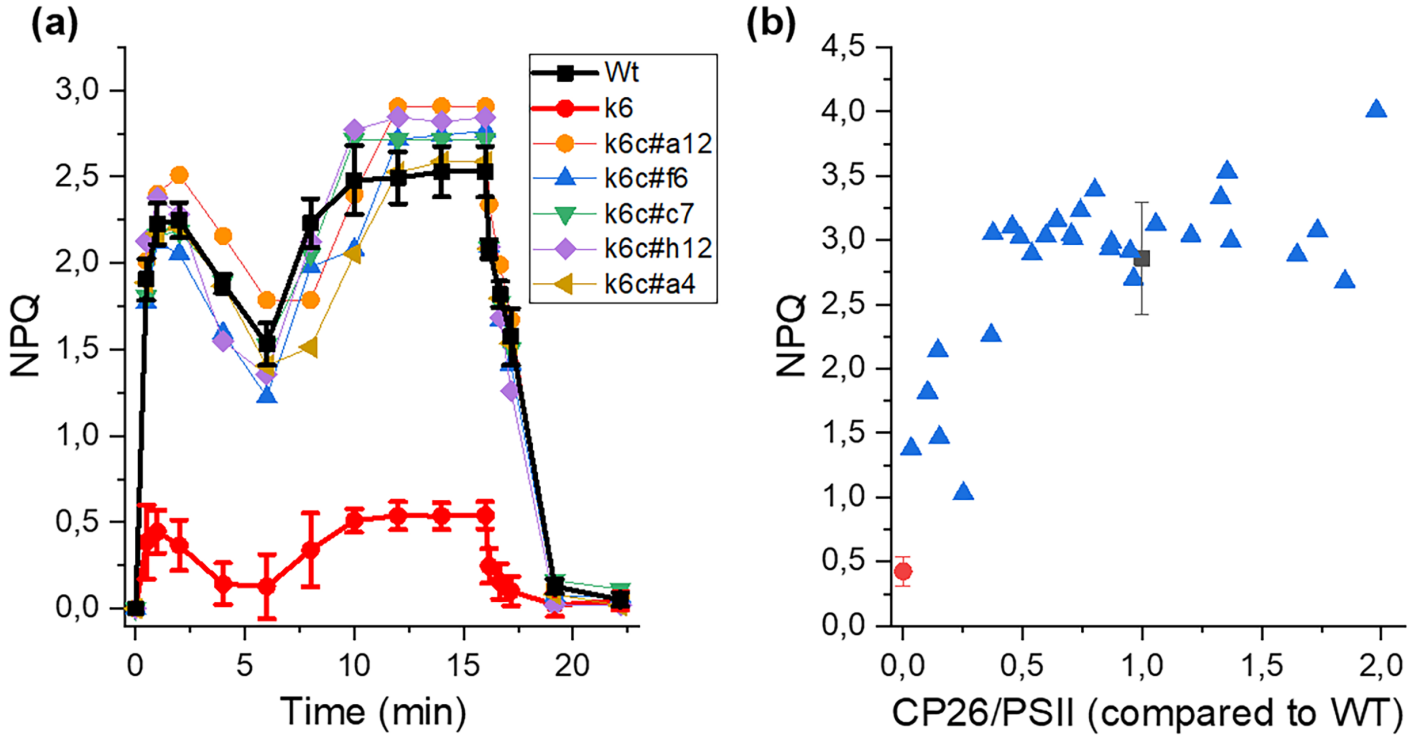

Figure 8. Nonphotochemical quenching in *k6* complemented line. (a) NPQ using an actinic light of 1,200 µmol m^{-2} s^{-1} in five *k6* lines complemented with CP26. The selected lines (named *k6c#*) accumulate CP26 to the same level as the wild-type. Wil-type (Wt, black) and k6 (red) NPQ was added as reference. (b) Correlation between the amount of CP26 and the NPQ reached after 15 minutes of illumination with actinic light at 1200 µmol m^{-2} s^{-1}. *k6c#* are indicate as blue triangles, Wt as a black square and *k6* as a red circle.

Parsed Citations

Albanese P, Melero R, Engel BD, Grinzato A, Berto P, Manfredi M, Chiodoni A, Vargas J, Sorzano CÓS, Marengo E, Saracco G, Zanotti G, Carazo J-M, Pagliano C (2017) Pea PSII-LHCII supercomplexes form pairs by making connections across the stromal gap. Scientific Reports 7: 10067

Google Scholar: Author Only Title Only Author and Title

Allorent G, Tokutsu R, Roach T, Peers G, Cardol P, Girard-Bascou J, Seigneurin-Berny D, Petroutsos D, Kuntz M, Breyton C, Franck F, Wollman FA, Niyogi KK, Krieger-Liszkay A, Minagawa J, Finazzi G (2013) A dual strategy to cope with high light in Chlamydomonas reinhardtii. Plant Cell 25: 545-557

Google Scholar: Author Only Title Only Author and Title

Aro E-M, Virgin I, Andersson B (1993) Photoinhibition of Photosystem II - inactivation, protein damage and turnover. Biochim.Biophys.Acta 1143: 113-134

Google Scholar: Author Only Title Only Author and Title

Baek K, Kim DH, Jeong J, Sim SJ, Melis A, Kim JS, Jin E, Bae S (2016) DNA-free two-gene knockout in Chlamydomonas reinhardtii via CRISPR-Cas9 ribonucleoproteins. Sci Rep 6: 30620

Google Scholar: Author Only Title Only Author and Title

Baker NR (2008) Chlorophyll fluorescence: a probe of photosynthesis in vivo. Annu.Rev.Plant Biol. 59: 89-113

Google Scholar: Author Only Title Only Author and Title

Ballottari M, Truong TB, De Re E, Erickson E, Stella GR, Fleming GR, Bassi R, Niyogi KK (2016) Identification of pH-sensing Sites in the Light Harvesting Complex Stress-related 3 Protein Essential for Triggering Non-photochemical Quenching in Chlamydomonas reinhardtii. J Biol Chem 291: 7334-7346

Google Scholar: Author Only Title Only Author and Title

Bernaerts T, Gheysen L, Foubert I, Hendrickx M, Van Loey A (2019) The potential of microalgae and their biopolymers as structuring ingredients in food: A review. Biotechnology Advances 37

Google Scholar: Author Only Title Only Author and Title

Bonente G, Howes BD, Caffarri S, Smulevich G, Bassi R (2008) Interactions between the photosystem II subunit PsbS and xanthophylls studied in vivo and in vitro. J Biol Chem 283: 8434-8445

Google Scholar: Author Only Title Only Author and Title

Butler WL (1973) Primary photochemistry of photosystem II in photosynthesis. Acc.Chem.Res. 6: 177-183

Google Scholar: Author Only Title Only Author and Title

Camacho F, Macedo A, Malcata F (2019) Potential Industrial Applications and Commercialization of Microalgae in the Functional Food and Feed Industries: A Short Review. Marine Drugs 17

Google Scholar: Author Only Title Only Author and Title

Cao P, Pan X, Su X, Liu Z, Li M (2020) Assembly of eukaryotic photosystem II with diverse light-harvesting antennas. Curr Opin Struct Biol 63: 49-57

Google Scholar: Author Only Title Only Author and Title

Cazzaniga S, Kim M, Bellamoli F, Jeong J, Lee S, Perozeni F, Pompa A, Jin E, Ballottari M (2020) Photosystem II antenna complexes CP26 and CP29 are essential for nonphotochemical quenching in Chlamydomonas reinhardtii. Plant Cell and Environment 43: 496-509

Google Scholar: Author Only Title Only Author and Title

Croce R, Van Amerongen H (2011) Light-harvesting and structural organization of Photosystem II: from individual complexes to thylakoid membrane. J.Photochem.Photobiol.B 104: 142-153

Google Scholar: Author Only Title Only Author and Title

Dall'Osto L, Cazzaniga S, Zappone D, Bassi R (2020) Monomeric light harvesting complexes enhance excitation energy transfer from LHCII to PSII and control their lateral spacing in thylakoids. Biochim Biophys Acta Bioenerg 1861: 148035

Google Scholar: Author Only Title Only Author and Title

de Bianchi S, Betterle N, Kouril R, Cazzaniga S, Boekema E, Bassi R, Dall'Osto L (2011) Arabidopsis mutants deleted in the light-harvesting protein Lhcb4 have a disrupted photosystem II macrostructure and are defective in photoprotection. Plant Cell 23: 2659-2679

Google Scholar: Author Only Title Only Author and Title

de Bianchi S, Dall'Osto L, Tognon G, Morosinotto T, Bassi R (2008) Minor antenna proteins CP24 and CP26 affect the interactions between photosystem II subunits and the electron transport rate in grana membranes of Arabidopsis. Plant Cell 20: 1012-1028

Google Scholar: Author Only Title Only Author and Title

Dinc E, Tian L, Roy LM, Roth R, Goodenough U, Croce R (2016) LHCSR1 induces a fast and reversible pH-dependent fluorescence quenching in LHCII in Chlamydomonas reinhardtii cells. Proc Natl Acad Sci U S A 113: 7673-7678
Google Scholar: Author Only Title Only Author and Title

Drop B, Webber-Birungi M, Yadav SK, Filipowicz-Szymanska A, Fusetti F, Boekema EJ, Croce R (2014) Light-harvesting complex II (LHCII) and its supramolecular organization in Chlamydomonas reinhardtii. Biochim Biophys Acta 1837: 63-72
Google Scholar: Author Only Title Only Author and Title

Elrad D, Niyogi KK, Grossman AR (2002) A major light-harvesting polypeptide of photosystem II functions in thermal dissipation. Plant Cell 14
Google Scholar: Author Only Title Only Author and Title

Erickson E, Wakao S, Niyogi KK (2015) Light stress and photoprotection in Chlamydomonas reinhardtii. Plant J 82: 449-465
Google Scholar: Author Only Title Only Author and Title

Garnier J, Maroc J, Guyon D (1986) Low-temperature fluorescence emission spectra and chlorophyll- protein complexes in mutants of Chlamydomonas reinhardtii: Evidence for a new chlorophyll-a-protein complex related to photosystem I. Biochim.Biophys.Acta 851: 395-406
Google Scholar: Author Only Title Only Author and Title

Genty B, Briantais J-M, Baker NR (1989) The relationship between the quantum yield of photosynthetic electron transport and quenching of chlorophyll fluorescence. Biochim.Biophys.Acta 990: 87-92
Google Scholar: Author Only Title Only Author and Title

Girolomoni L, Ferrante P, Berteotti S, Giuliano G, Bassi R, Ballottari M (2017) The function of LHCBM4/6/8 antenna proteins in Chlamydomonas reinhardtii. J Exp Bot 68: 627-641
Google Scholar: Author Only Title Only Author and Title

Graham PJ, Nguyen B, Burdyny T, Sinton D (2017) A penalty on photosynthetic growth in fluctuating light. Sci Rep 7: 12513
Google Scholar: Author Only Title Only Author and Title

Głowacka K, Kromdijk J, Kucera K, Xie J, Cavanagh AP, Leonelli L, Leakey ADB, Ort DR, Niyogi KK, Long SP (2018) Photosystem II Subunit S overexpression increases the efficiency of water use in a field-grown crop. Nat Commun 9: 868
Google Scholar: Author Only Title Only Author and Title

Hill R, Scarisbrick R (1940) Production of Oxygen by Illuminated Chloroplasts. Nature 146: 61
Google Scholar: Author Only Title Only Author and Title

Horton P (1996) Nonphotochemical quenching of chlorophyll fluorescence. In RC Jennings, ed, Light as an Energy Source and Information Carrier in Plant Physiology. New York, Plenum Press, pp 99-111
Google Scholar: Author Only Title Only Author and Title

Hyams J, Davies DR (1972) The induction and characterisation of cell wall mutants of Chlamydomonas reinhardi. Mutation Research/Fundamental and Molecular Mechanisms of Mutagenesis 14: 381-389
Google Scholar: Author Only Title Only Author and Title

Joo S, Kariyawasam T, Kim M, Jin E, Goodenough U, Lee JH (2022) Sex-linked deubiquitinase establishes uniparental transmission of chloroplast DNA. Nat Commun 13: 1133
Google Scholar: Author Only Title Only Author and Title

Kim E, Akimoto S, Tokutsu R, Yokono M, Minagawa J (2017) Fluorescence lifetime analyses reveal how the high light-responsive protein LHCSR3 transforms PSII light-harvesting complexes into an energy-dissipative state. J Biol Chem 292: 18951-18960
Google Scholar: Author Only Title Only Author and Title

Kim E, Watanabe A, Duffy CDP, Ruban AV, Minagawa J (2020) Multimeric and monomeric photosystem II supercomplexes represent structural adaptations to low- and high-light conditions. J Biol Chem 295: 14537-14545
Google Scholar: Author Only Title Only Author and Title

Kim J, Lee S, Baek K, Jin E (2020) Site-Specific Gene Knock-Out and On-Site Heterologous Gene Overexpression in Chlamydomonas reinhardtii via a CRISPR-Cas9-Mediated Knock-in Method. Front Plant Sci 11: 306
Google Scholar: Author Only Title Only Author and Title

Koyande A, Chew K, Rambabu K, Tao Y, Chu D, Show P (2019) Microalgae: A potential alternative to health supplementation for humans. Food Science and Human Wellness 8: 16-24
Google Scholar: Author Only Title Only Author and Title

Kromdijk J, Glowacka K, Leonelli L, Gabilly ST, Iwai M, Niyogi KK, Long SP (2016) Improving photosynthesis and crop productivity by accelerating recovery from photoprotection. Science 354: 857-861
Google Scholar: Author Only Title Only Author and Title

Kropat J, Hong-Hermesdorf A, Casero D, Ent P, Castruita M, Pellegrini M, Merchant S, Malasarn D (2011) A revised mineral

nutrient supplement increases biomass and growth rate in Chlamydomonas reinhardtii. Plant Journal 66: 770-780
Google Scholar: Author Only Title Only Author and Title

Lagarde D, Beuf L, Vermaas W (2000) Increased production of zeaxanthin and other pigments by application of genetic engineering techniques to Synechocystis sp. strain PCC 6803. Appl Environ Microbiol 66: 64-72
Google Scholar: Author Only Title Only Author and Title

Liguori N, Novoderezhkin V, Roy LM, van Grondelle R, Croce R (2016) Excitation dynamics and structural implication of the stress-related complex LHCSR3 from the green alga Chlamydomonas reinhardtii. Biochim Biophys Acta 1857: 1514-1523
Google Scholar: Author Only Title Only Author and Title

Liguori N, Roy LM, Opacic M, Durand G, Croce R (2013) Regulation of light harvesting in the green alga Chlamydomonas reinhardtii: the C-terminus of LHCSR is the knob of a dimmer switch. J Am Chem Soc 135: 18339-18342
Google Scholar: Author Only Title Only Author and Title

Long SP, Humphries S, Falkowski PG (1994) Photoinhibition of photosynthesis in nature. Ann.Rev.Plant Physiol.Plant Mol.Biol. 45: 633-662
Google Scholar: Author Only Title Only Author and Title

Malkin S, Armond PA, Mooney HA, Fork DC (1981) Photosystem II Photosynthetic Unit Sizes from Fluorescence Induction in Leaves : CORRELATION TO PHOTOSYNTHETIC CAPACITY. Plant Physiol 67: 570-579
Google Scholar: Author Only Title Only Author and Title

Medipally SR, Yusoff FM, Banerjee S, Shariff M (2015) Microalgae as Sustainable Renewable Energy Feedstock for Biofuel Production. Biomed Res Int 2015: 519513
Google Scholar: Author Only Title Only Author and Title

Minagawa J, Takahashi Y (2004) Structure, function and assembly of Photosystem II and its light-harvesting proteins. Photosynth Res 82: 241-263
Google Scholar: Author Only Title Only Author and Title

Natali A, Croce R (2015) Characterization of the major light-harvesting complexes (LHCBM) of the green alga Chlamydomonas reinhardtii. PLoS One 10: e0119211
Google Scholar: Author Only Title Only Author and Title

Neidhardt J, Benemann JR, Zhang LP, Melis A (1998) Photosystem-II repair and chloroplast recovery from irradiance stress: relationship between chronic photoinhibition, light-harvesting chlorophyll antenna size and photosynthetic productivity in Dunaliella salina (green algae). Photosynthesis Research 56: 175-184
Google Scholar: Author Only Title Only Author and Title

Nelson N, Ben Shem A (2004) The complex architecture of oxygenic photosynthesis. Nature 5: 1-12
Google Scholar: Author Only Title Only Author and Title

Niyogi KK, Truong TB (2013) Evolution of flexible non-photochemical quenching mechanisms that regulate light harvesting in oxygenic photosynthesis. Curr Opin Plant Biol 16: 307-314
Google Scholar: Author Only Title Only Author and Title

Peers G, Truong TB, Ostendorf E, Busch A, Elrad D, Grossman AR, Hippler M, Niyogi KK (2009) An ancient light-harvesting protein is critical for the regulation of algal photosynthesis. Nature 462: 518-521
Google Scholar: Author Only Title Only Author and Title

Perozeni F, Cazzaniga S, Baier T (2020) Turning a green alga red: engineering astaxanthin biosynthesis by intragenic pseudogene revival in Chlamydomonas reinhardtii. 18: 2053-2067
Google Scholar: Author Only Title Only Author and Title

Perozeni F, Cazzaniga S, Baier T, Zanoni F, Zoccatelli G, Lauersen K, Wobbe L, Ballottari M (2020) Turning a green alga red: engineering astaxanthin biosynthesis by intragenic pseudogene revival in Chlamydomonas reinhardtii. Plant Biotechnology Journal 18: 2053-2067
Google Scholar: Author Only Title Only Author and Title

Peter GF, Takeuchi T, Thornber JP (1991) Solubilization and two-dimensional electrophoretic procedures for studying the organization and composition of photosynthetic membrane polypeptides. Methods: A Companion to Methods in Enzymology 3: 115-124
Google Scholar: Author Only Title Only Author and Title

Rani A, Saini KC, Bast F, Mehariya S, Bhatia SK, Lavecchia R, Zuorro A (2021) Microorganisms: A Potential Source of Bioactive Molecules for Antioxidant Applications. Molecules 26
Google Scholar: Author Only Title Only Author and Title

Sacharz J, Giovagnetti V, Ungerer P, Mastroianni G, Ruban AV (2017) The xanthophyll cycle affects reversible interactions

between PsbS and light-harvesting complex II to control non-photochemical quenching. Nat Plants 3: 16225
Google Scholar: Author Only Title Only Author and Title

Schägger H, von Jagow G (1987) Tricine-sodium dodecyl sulfate-polyacrylamide gel electrophoresis for the separation of proteins in the range from 1 to 100 kDa. Anal.Biochem. 166: 368-379
Google Scholar: Author Only Title Only Author and Title

Semchonok DA, Sathish Yadav KN, Xu P, Drop B, Croce R, Boekema EJ (2017) Interaction between the photoprotective protein LHCSR3 and C2S2 Photosystem II supercomplex in Chlamydomonas reinhardtii. Biochim Biophys Acta 1858: 379-385
Google Scholar: Author Only Title Only Author and Title

Shen L, Huang Z, Chang S, Wang W, Wang J, Kuang T, Han G, Shen J-R, Zhang X (2019) Structure of a C2S2M2N2-type PSII–LHCII supercomplex from the green alga Chlamydomonas reinhardtii. Proceedings of the National Academy of Sciences 116: 21246-21255
Google Scholar: Author Only Title Only Author and Title

Suga M, Akita F, Hirata K, Ueno G, Murakami H, Nakajima Y, Shimizu T, Yamashita K, Yamamoto M, Ago H, Shen JR (2015) Native structure of photosystem II at 1.95 A resolution viewed by femtosecond X-ray pulses. Nature 517: 99-103
Google Scholar: Author Only Title Only Author and Title

Tian L, Nawrocki Wojciech J, Liu X, Polukhina I, van Stokkum Ivo HM, Croce R (2019) pH dependence, kinetics and light-harvesting regulation of nonphotochemical quenching in Chlamydomonas. Proceedings of the National Academy of Sciences 116: 8320-8325
Google Scholar: Author Only Title Only Author and Title

Tokutsu R, Kato N, Bui KH, Ishikawa T, Minagawa J (2012) Revisiting the supramolecular organization of photosystem II in Chlamydomonas reinhardtii. J Biol Chem 287: 31574-31581
Google Scholar: Author Only Title Only Author and Title

Tokutsu R, Minagawa J (2013) Energy-dissipative supercomplex of photosystem II associated with LHCSR3 in Chlamydomonas reinhardtii. Proc Natl Acad Sci U S A 110: 10016-10021
Google Scholar: Author Only Title Only Author and Title

Troiano JM, Perozeni F, Moya R, Zuliani L, Baek K, Jin E, Cazzaniga S, Ballottari M, Schlau-Cohen GS (2021) Identification of distinct pH- and zeaxanthin-dependent quenching in LHCSR3 from Chlamydomonas reinhardtii. Elife 10
Google Scholar: Author Only Title Only Author and Title

Van Kooten O, Snel JFH (1990) The use of chlorophyll fluorescence nomenclature in plant stress physiology. Photosynt.Res. 25: 147-150
Google Scholar: Author Only Title Only Author and Title

Vass I, Styring S, Hundal T, Koivuniemi A, Aro E-M, Andersson B (1992) Reversible and irreversible intermediates during photoinhibition of photosystem II: Stable reduced QA species promote chlorophyll triplet formation. Proc.Natl.Acad.Sci.USA 89: 1408-1412
Google Scholar: Author Only Title Only Author and Title

ACKNOWLEDGEMENTS

The research was supported by the ERC (European Research Council) Starting Grant SOLENALGAE (679814) to M.B. and by Basic Science Research Program (NRF2020R1A2C2011998) and Carbon to X Project (2020M3H7A1098294) of the National Research Foundation (NRF) of Korea, funded by the Korean government. to E.J.

AUTHOR CONTRIBUTIONS

MB designed the research. EJ coordinated the research activity for generation of mutant strains and contributed to experiment design. CD coordinated the research activity for time resolved fluorescence analysis of whole cells. SC, MK, SS, FP and MP performed experiments. All the authors analyzed data. SC, EJ and MB wrote the paper. All the authors discussed the results, contributed to data interpretation, commented on the manuscript and approved its final version.

Authors declare no conflict of interest